British Journal of Pharmacology

DOI:10.1111/j.1476-5381.2012.01987.x
www.brjpharmacol.org

RESEARCH PAPER

Positive allosteric modulation by ivermectin of human but not murine P2X7 receptors

W Nörenberg[1], H Sobottka[1], C Hempel[1], T Plötz[1], W Fischer[1], G Schmalzing[2] and M Schaefer[1]

[1]*Rudolf-Boehm-Institute of Pharmacology and Toxicology, Medical Faculty, University of Leipzig, Leipzig, Germany, and* [2]*Department of Molecular Pharmacology, RWTH Aachen University, Aachen, Germany*

Correspondence
M Schaefer, Department of Pharmacology and Toxicology, Medical Faculty, University of Leipzig, Härtelstr. 16-18, 04107 Leipzig, Germany. E-mail: michael.schaefer@medizin.uni-leipzig.de

Keywords
purinergic signalling; ATP pharmacology; ligand-gated channel; pore dilation; ivermectin; P2X4; P2X7; species differences

Received
4 January 2012
Revised
5 March 2012
Accepted
14 March 2012

BACKGROUND AND PURPOSE

In mammalian cells, the anti-parasitic drug ivermectin is known as a positive allosteric modulator of the ATP-activated ion channel P2X4 and is used to discriminate between P2X4- and P2X7-mediated cellular responses. In this paper we provide evidence that the reported isoform selectivity of ivermectin is a species-specific phenomenon.

EXPERIMENTAL APPROACH

Complementary electrophysiological and fluorometric methods were applied to evaluate the effect of ivermectin on recombinantly expressed and on native P2X7 receptors. A biophysical characterization of ionic currents and of the pore dilation properties is provided.

KEY RESULTS

Unexpectedly, ivermectin potentiated currents in human monocyte-derived macrophages that endogenously express hP2X7 receptors. Likewise, currents and $[Ca^{2+}]_i$ influx through recombinant human (hP2X7) receptors were potently enhanced by ivermectin at submaximal or saturating ATP concentrations. Since intracellular ivermectin did not mimic or prevent its activity when applied to the bath solution, the binding site of ivermectin on hP2X7 receptors appears to be accessible from the extracellular side. In contrast to currents through P2X4 receptors, ivermectin did not cause a delay in hP2X7 current decay upon ATP removal. Interestingly, $NMDG^+$ permeability and Yo-Pro-1 uptake were not affected by ivermectin. On rat or mouse P2X7 receptors, ivermectin was only poorly effective, suggesting a species-specific mode of action.

CONCLUSIONS AND IMPLICATIONS

The data indicate a previously unrecognized species-specific modulation of human P2X7 receptors by ivermectin that should be considered when using this cell-biological tool in human cells and tissues.

Abbreviations

$[Ca^{2+}]_i$, intracellular free Ca^{2+} concentration; 5-BDBD (5-(3-bromophenyl)-1,3-dihydro-2*H*-benzofuro[3,2-*e*]-1,4-diazepin-2-one); A 438079, 3-[[5-(2,3-dichlorophenyl)-1*H*-tetrazoyl-1-yl]methyl]pyridine; AZ 10606120, *N*-[2-[[2-[(2-hydroxyethyl) amino]ethyl]amino]-5-quinolinyl]-2-tricyclo[3.3.1.13,7]de-1-ylacetamide; BzATP, 2′(3′)-*O*-(4-benzolybenzoyl)adenosine-5′-triphosphate; DIC, divalent cations; GluCl, glutamate-gated chloride channel; HBS, HEPES-buffered solution; hMDM, human monocyte-derived macrophages; *I*, ionic current; $NMDG^+$, *N*-methyl-D-glucamine; P_{NMDG}/P_{Na}, permeability ratio for $NMDG^+$ with respect to Na^+; TM, transmembrane; V_c, command potential; V_{rev}, reversal potential

Introduction

Purine-mediated signalling is an almost ubiquitous phenomenon, involving several classes of G-protein-coupled (P2Y) or ion channel-coupled (P2X) receptors (nomenclature follows Alexander *et al.*, 2011). The latter, also referred to as ionotropic or ligand-gated P2X receptors, comprise seven genes, whose gene products P2X1–P2X7 consist of a long extracellular loop (~280 amino acids) and two transmembrane (TM)-spanning segments with intracellularly located N and C termini of variable length, and assemble to form homo- or heterotrimeric complexes with a central ion-conducting pore (Khakh and North, 2006; Coddou *et al.*, 2011). ATP binding to P2X receptors triggers channel opening, giving rise to poorly selective cation currents. Depending on the cell type, P2X receptor activation triggers diverse cell-biological responses, including smooth muscle contraction, neuronal depolarization, chemotaxis, immune cell activation, cell proliferation or apoptosis (Burnstock and Verkhratsky, 2010; Burnstock and Kennedy, 2011; Junger, 2011). In addition, prolonged or repetitive agonist application to P2X2, P2X4 and P2X7 receptors promotes the formation of large pores allowing the passage of organic cations of up to 900 Da (Khakh *et al.*, 1999a; North, 2002).

Ionic currents that are mediated by distinct homo- or heterotrimeric P2X receptor complexes can be discriminated based on their ATP sensitivity, inactivation properties and pharmacological modulation (Coddou *et al.*, 2011). In the presence of physiological extracellular concentrations of divalent cations Mg^{2+} and Ca^{2+} (standard DIC), P2X7 receptors require millimolar ATP concentrations to become fully activated. In low divalent cation concentrations (low DIC), P2X7 receptors are released from a Ca^{2+}-dependent allosteric block, resulting in higher ATP binding affinity and markedly increased current amplitudes (Yan *et al.*, 2011).

As many cell types co-express two or more P2X receptor isoforms, as well as one or more P2Y receptors, there is a need for selective pharmacological compounds. Specific blockers are available for some, but not all P2X receptor isoforms (Jarvis and Khakh, 2009; Coddou *et al.*, 2011) and specifically acting organic blockers of P2X7, as well as P2X2 receptors have been described (Guile *et al.*, 2009; Jarvis and Khakh, 2009). However, specific P2X4 receptor blockers are not available. Only recently, 5-(3-bromophenyl)-1,3-dihydro-2*H*-benzofuro[3,2-*e*]-1,4-diazepin-2-one (5-BDBD) has been developed and described as a P2X4 receptor-specific compound (Donnelly-Roberts *et al.*, 2008; Wu *et al.*, 2011). Up to that time, most pharmacological attempts to identify P2X4 channels have relied on the observation that the responses of these channels can be potentiated by low micromolar concentrations of Zn^{2+} (Wildman *et al.*, 1999; Coddou *et al.*, 2007) or by the macrocyclic lactone antibiotic ivermectin (Khakh *et al.*, 1999b).

Ivermectin irreversibly activates a glutamate-gated chloride channel receptor that is present in nematodes and some arthropods but not in vertebrates (Cully *et al.*, 1994). In mammals, ivermectin has been shown to potentiate P2X4 receptor-mediated signalling. Ivermectin binding to P2X4 receptors presumably involves interaction with the transmembrane-spanning helices 1 and 2. Thus, at least one of the ivermectin binding sites is buried in the plasma membrane and directly affects channel gating (Silberberg *et al.*, 2007; Jelínkova *et al.*, 2008). In the presence of ivermectin, P2X4 currents display a massive delay of current deactivation after ATP wash-out. In the continuous presence of ATP, maximal current amplitudes and the ATP sensitivity are increased (Khakh *et al.*, 1999b). At the level of unitary currents, ivermectin augments the single channel conductance, prolongs the mean open times and facilitates a burst-like activity pattern, culminating in the potentiating effect that is observed in the whole cell configuration (Priel and Silberberg, 2004).

The original description of ivermectin potentiation of P2X4 receptors provided evidence for a P2X4-selective mode of action by demonstrating that no effects are elicited on P2X2, P2X3, P2X2:P2X3 receptor heteromers or P2X7 receptors (Khakh *et al.*, 1999b). Since then, potentiation by ivermectin of ATP-triggered currents has been interpreted as evidence for the involvement of P2X4 receptors.

Unexpected findings in human macrophages that endogenously co-express P2X4 and P2X7 receptors (Guo *et al.*, 2007) prompted us to re-evaluate the specificity profile of ivermectin, leading to the observation that ivermectin can no longer be considered a P2X4 receptor subtype-specific tool in human cells and tissues. Nonetheless, we confirmed the initial observation of P2X4 subtype specificity in rodent P2X receptors and concluded that ivermectin adds to the growing list of species-specific allosteric modulators of P2X7 receptors (Michel *et al.*, 2009; Coddou *et al.*, 2011).

Methods

Cell culture

HEK 293 cells stably transfected with the human P2X7 (hP2X7) receptor (HEK_{hP2X7}) were cultured as described (Nörenberg *et al.*, 2011) and used for experimentation 2 days after splitting. Similarly, human P2X4 was stably transfected in a HEK_{hP2X4} cell line, selected and expanded in a culturing medium containing 600 $\mu g \cdot mL^{-1}$ geniticin. The rat P2X7 (rP2X7) was stably and inducibly expressed in a Flp-in T-REx HEK293 cell line (Invitrogen, Karlsruhe, Germany), selected in the presence of 15 $\mu g \cdot mL^{-1}$ blasticidine and 100 $\mu g \cdot mL^{-1}$ hygromycin. The expression of rP2X7 was induced by supplementing the culturing medium with 1 $\mu g \cdot mL^{-1}$ tetracycline 18–24 h prior to the experiments.

Human blood samples were taken from healthy volunteers, using procedures approved by the local ethical committee. Human monocyte-derived macrophages (hMDM) were prepared and cultured as described by Davies and Gordon (2005), with minor modifications. Briefly, monocytes were isolated from buffy coat fractions by a one-step density gradient centrifugation (Histopaque 1077, Sigma-Aldrich, St. Louis, MO). After washing with ice-cold PBS, containing no Ca^{2+} and Mg^{2+}, cells were re-suspended in RPMI-1640 medium (PAA, Pasching, Austria) with 10% autologous fibrin-depleted plasma, 2 mM L-glutamine, non-essential amino acids, 1 mM sodium pyruvate, 100 $mg \cdot mL^{-1}$ streptomycin and 100 $U \cdot mL^{-1}$ penicillin (complete RPMI). Cells were allowed to differentiate spontaneously into macrophages during 5–7 days in culture.

All experimental procedures involving animals were approved by the Committee on Animal Care and Use of the local governmental body. Procedures were optimized to reduce the number of animals and their suffering, according to the regulations of the German Animal Welfare Act. All studies involving animals are reported in accordance with the ARRIVE guidelines for reporting experiments involving animals (McGrath *et al.*, 2010). A total of 12 rats and 8 mice were used in the experiments described here.

Astrocyte-enriched cultures were obtained following the protocol of Vermeiren *et al*. (2005). Brains from newborn Wistar rats or C57BL/6 mice were dissected under sterile conditions. Isolated cortices were freed of meninges and blood vessels, minced and then gently triturated through a fire-polished Pasteur pipette in DMEM plus 2.5 mM L-alanyl-L-glutamin (Invitrogen), supplemented with 10% fetal calf serum (FCS; Seromed, Berlin, Germany), proline (50 $\mu g \cdot mL^{-1}$), D-glucose (36 mM), HEPES (15 mM, pH 7.4 with NaOH) and gentamycin (50 $\mu g \cdot mL^{-1}$; all Sigma-Aldrich, Taufkirchen, Germany). After centrifugation and washing twice at 984× *g* for 5 min, remaining cell pellets were re-suspended in culture medium, seeded in poly-L-lysine-coated (Sigma) culture flasks (Greiner Bio-One, Frickenhausen, Germany) and maintained at 37°C in a humidified incubator gassed with 5% CO_2. After 7 days, oligodendrocytes were removed by medium exchange after agitating at 80 rpm for 6 h on an orbital shaker. Three days later, cells were detached with PBS containing 0.25% trypsin (Invitrogen) and 1 mM EDTA (Sigma), poured into poly-L-lysine-coated 35 mm diameter culture dishes (Greiner Bio-One) at a density of about 5×10^3 cells cm^{-2} and allowed to settle for 24 h. In order to eliminate microglial contamination, L-leucine methyl ester (5 mM; Sigma) was added (Giulian and Baker, 1986). Cell differentiation and *in vitro* activation of astrocytes (Vermeiren *et al*., 2005) were initiated by reducing the FCS content in the medium to 3%, followed by supplementation with 5 $\mu g \cdot mL^{-1}$ insulin, 50 $\mu g \cdot mL^{-1}$ human transferrin, 5.2 $ng \cdot mL^{-1}$ selenite, 1 $\mu g \cdot mL^{-1}$ biotin, 3.6 $ng \cdot mL^{-1}$ hydrocortisone, 5 $ng \cdot mL^{-1}$ basic fibroblast growth factor and 1 $ng \cdot mL^{-1}$ EGF (G5 culture additive; Gibco, Karlsruhe, Germany). Astroglial cells were used for experiments 5–6 days after lowering FCS and/or adding G5.

Fluorimetric $[Ca^{2+}]_i$ measurement

For calcium imaging, HEK_{hP2X7} cells were harvested with trypsin and incubated with fluo-4/AM (4 μM; Molecular Probes Invitrogen) at 37°C for 30 min in culture medium. Loaded cell suspensions were washed again and re-suspended into a HEPES-buffered solution (HBS), containing 130 mM NaCl, 10 mM HEPES, 6 mM KCl, 1 mM $CaCl_2$, 1 mM $MgCl_2$, 5.5 mM D-glucose, adjusted to pH 7.4 with NaOH. The cell suspension was dispensed into black pigmented, clear-bottomed 384 microtitre plates (low-binding; Corning, Lowell, MA).

Measurements were made using a custom-made fluorescence plate imaging device built into a robotic liquid handling station (Freedom Evo 150, Tecan, Switzerland). The plate imaging device comprises a 460 nm LED array, filtered with a 475 nm short-pass filter (DT-blue; Optic Balzers, Oerlikon, Switzerland) and a cooled CCD camera (Coolsnap FX, Photometrics, Tucson, AZ), equipped with a Xenon 0.95/25 C mount lens (Schneider Kreuznach, Bad Kreuznach, Germany) and a 515 nm long-pass filter (Y515-Di; Fujifilm, Tokyo, Japan). The imaging was controlled with the Micromanager software (Edelstein *et al*., 2010). Fluorescence intensities were monitored during sequential injection of various concentrations of the modulators and ATP using the 96-tip multichannel arm of the liquid handling device. The fluorescence intensity in single wells was calculated (imageJ; Abramoff *et al*., 2004), corrected for the respective background signals and normalized to the initial intensities (F/F_0) to compensate for uneven loading and fluorescence detection sensitivity. Concentration–response functions were constructed by non-linear regression analysis.

Yo-Pro-1 uptake assay

The permeability of large organic molecules was monitored using a Yo-Pro-1 accumulation assay. Cells were harvested, washed and re-suspended in HBS with low divalent cation concentrations (no $MgCl_2$ and 0.1 mM $CaCl_2$; low-DIC HBS). Yo-Pro-1 (1 μM; Invitrogen) was added; cells were dispensed into 384-well microtitre plates. The fluorescence was monitored in a filter-based plate reader system (Polarstar Omega, BMG Labtech, Offenburg, Germany) with 485 ± 6 and 529 ± 10 nm band-pass filters for excitation and emission respectively.

Electrophysiology

Whole-cell recordings were made at room temperature and at a holding potential of −60 mV, using an EPC9 amplifier and Pulse software (HEKA, Lambrecht, Germany). The extracellular solution for seal formation (standard divalent cation concentration-containing bath = standard DIC), also used during some of the experiments, contained 147 mM NaCl, 2 mM KCl, 2 mM $CaCl_2$, 1 mM $MgCl_2$, 13 mM D-glucose and 10 mM HEPES (~305 $mOsm \cdot L^{-1}$; pH 7.3 with NaOH). Unless otherwise stated, cells were superfused, after the whole-cell configuration had been achieved, with a low divalent cation-containing bath solution (low DIC), differing from the standard DIC solution by the omission of $MgCl_2$ and a lower $CaCl_2$ content of 0.1 mM. In experiments with astroglial cells, the low DIC bath solution also contained carbenoxolone (100 μM) in order to block gap junction-like conductances. The pipette solution comprised in both cases (low or standard DIC) 147 mM KCl, 10 mM HEPES and 10 mM EGTA (~300 $mOsm \cdot L^{-1}$; pH 7.3 with KOH). Effects of ivermectin on hP2X7 pore dilation were assessed with a bath solution containing *N*-methyl-D-glucamine ($NMDG^+$, 154 mM), HEPES (10 mM) and D-glucose (13 mM; ~310 $mOsm \cdot L^{-1}$, pH 7.3 with HCl). The respective pipette solution included 147 mM NaCl, 10 mM HEPES and 10 mM EGTA (~310 $mOsm \cdot L^{-1}$, pH 7.3 with NaOH). When filled with one of the above pipette solutions, patch pipettes for whole-cell recordings had a resistance of 2–4 MΩ. Drugs were focally delivered by means of the application cannula (100 μm inner diameter) of a solenoid valve-driven pressurized superfusion system (DAD-12, Adams and List, New York, NY), placed in the vicinity (~50 μm) of the cell under investigation. Series resistance (8–20 MΩ) was compensated by 60–80%. Experiments during which series resistance changed by more than 20% were not included in the analysis. ATP-induced currents, sampled at 5 kHz and filtered at 1.7 kHz, were measured as peak responses with

respect to the holding current level. They were normalized for differences in cell size (membrane capacitance) to obtain current densities (pA pF^{-1}). Calculation of permeability ratio for $NMDG^+$ with respect to Na^+ (P_{NMDG}/P_{Na}) was made by assuming ion activities of 0.75 for both cations and using a modified Goldman-Hodgkin-Katz equation of the form $P_{NMDG}/P_{Na} = ([Na]_i/[NMDG]_o)\ exp^{(Vrev\ F/R\ T)}$, where $[Na]_i$ and $[NMDG]_o$ are the concentrations of Na^+ and $NMDG^+$ in the intracellular- and extracellular solution, respectively; F is the Faraday constant; R is the universal gas constant; and T is the absolute temperature.

Statistical analysis

Results are expressed as means ± SEM, obtained in n cells (electrophysiology) or fluorometric experiments. Differences in means were tested for significance by the Mann–Whitney U-test or by the Kruskal–Wallis one-way ANOVA on ranks followed by a modified Student's t-test (Bonferroni–Dunn) in the case of single and multiple comparisons respectively. $P < 0.05$ was the accepted minimum level of significance. Concentration response functions were fitted to a Hill equation: $E = E_{min} + (E_{max} - E_{min})/(1 + ([M]/EC_{50})^{-nH})$. E_{min} and E_{max} are the extrapolated minimum and maximum effects with no modulator or with saturating modulator concentrations, [M] is the actual concentration of the modulator, EC_{50} is the modulator concentration producing 50% of the concentration-dependent effect and nH is the Hill coefficient that indicated the cooperativity of the effect. In experiments that revealed biphasic response properties, the sum of two Hill equations was applied to model the data. Mono- and bi-exponential fits of current rise or decay kinetics were performed by applying the functions $I_{ATP(t)} = A_o + A_1\ exp^{(-t/\tau)}$ and $I_{ATP(t)} = A_o + A_1\ exp^{(-t/\tau_{fast})} + A_2\ exp^{(-t/\tau_{slow})}$ respectively. The time constants τ, τ_{fast} and τ_{slow} are obtained by nonlinear curve fitting. A_0 and A_1 or A_2 denote the detected initial signal level at $t = 0$ s and the extrapolated effect level at infinite time respectively. All nonlinear fitting procedures were performed using the Levenberg–Marquardt algorithm.

Materials

ATP, carbenoxolone and clemastine were from Sigma-Aldrich. 3-[[5-(2,3-dichlorophenyl)-1*H*-tetrazoyl-1-yl]methyl]pyridine (A 438079), *N*-[2-[[2-[(2-hydroxyethyl)amino]ethyl]amino]-5-quinolinyl]-2-tricyclo[3.3.1.13,7]de-1-ylacetamide (AZ 10606120), 5-BDBD, 2′(3′)-*O*-(4-benzolybenzoyl)adenosine-5′-triphosphate (BzATP) and ivermectin were from Tocris (Bristol, UK). Stock solutions of drugs (1–100 mM) were prepared with the appropriate standard or low DIC bath solution (ATP and clemastine), deionized water (carbenoxolone) or DMSO (A 438079, AZ 10606120, 5-BDBD and ivermectin). With the exception of carbenoxolone, which was always freshly prepared at the experimental day, aliquots of stock solutions were stored at –20°C and freshly diluted with the appropriate extracellular saline. The final DMSO concentration in the bath never exceeded 0.1%, a concentration that had no effect on ATP-induced currents in hMDM or HEK_{hP2X7} cells. ATP and clemastine stock solutions were routinely readjusted to pH 7.3.

Results

Ivermectin enhances non-inactivating P2X7-like currents in human macrophages

Macrophages functionally co-express at least three members of the P2X receptor family: P2X1, P2X4 and P2X7 (Brône *et al.*, 2007). In hMDM, a rapidly inactivating P2X1-like component of ATP-triggered inward currents was observed in 27 out of 42 cells and completely desensitized by a repeated stimulation regime (e.g. Figure 1A). In contrast, a non-inactivating, P2X7-like current developed within six to seven repetitions of ATP exposure (6 s each, applied at 2 min intervals), reaching steady-state current densities of 6.0 ± 1.1 pA·pF^{-1} ($n = 42$). The non-inactivating kinetics, the sensitization during repetitive agonist application and the inhibition by the P2X7 receptor blocker A 438097 of ATP-triggered currents in hMDM suggested a dominant contribution of P2X7, rather than P2X4 receptors (Nörenberg *et al.*, 2011). Nevertheless, we noted that acute application of ivermectin reversibly potentiated the current amplitudes by 35.0 ± 4.2% ($n = 11$) compared with respective solvent controls (DMSO 0.1%; Figure 1A,B right panel, Figure 1F). Intriguingly, incubation with the P2X4 receptor blocker 5-BDBD diminished the current amplitudes only by a small amount (Figure 1C,E), and ivermectin still potentiated the remaining current by 22.1% ± 4.2% ($n = 7$; Figure 1C,F). We therefore concluded that either 5-BDBD was poorly efficient in blocking P2X4 receptors or that the most prominent part of the current is carried by P2X7 receptors, and ivermectin may exert an unexpected potentiation of this P2X7 component. Applying the P2X7 receptor blocker A 438079, we found a more pronounced reduction of current amplitudes with the remaining current again being slightly (16.5% ± 2.9%; $n = 7$) but not significantly potentiated by ivermectin (Figure 1D–F). The combination of 5-BDBD with A 438079 yielded an additive block of the ATP-induced currents and abolished the potentiating effect of ivermectin (Figure 1E,F).

In order to ensure the effectiveness of 5-BDBD, we tested the inhibitor using a HEK cell line that stably expresses human P2X4 (HEK_{hP2X4}). In the presence of 3 μM ivermectin, this cell line displayed the typical potentiation and delayed inactivation during ATP washout. In contrast, no current potentiation or delay in inactivation was elicited by 30 μM clemastine (Figure S1). At a concentration of 5 μM, 5-BDBD treatment suppressed hP2X4 current amplitudes by about 70%, whereas the P2X7 receptor-specific blocker A 438079 did not significantly inhibit hP2X4 receptors when applied at 10 μM (Figure 2A–C). *Vice versa*, stably expressed human P2X7 (hP2X7) receptors were almost completely suppressed by 10 μM A 438079 (see Figure 2D,F) and irreversibly blocked by the highly potent, non-competitive P2X7 receptor blocker AZ 10606120 at a concentration of 0.3 μM (data not shown). In contrast, 5 μM 5-BDBD did not significantly affect hP2X7 current amplitudes (Figure 2D,F). Thus, the receptor blockers were sufficiently selective and active, and the possibility that ivermectin may have an augmenting effect on hP2X7 currents could not be ruled out. To test this hypothesis directly, the hP2X7 receptor-expressing cell line was exposed to 3 μM ivermectin either in a bath solution that contained 1 mM $MgCl_2$ and 2 mM $CaCl_2$ (standard DIC) or low extracellular

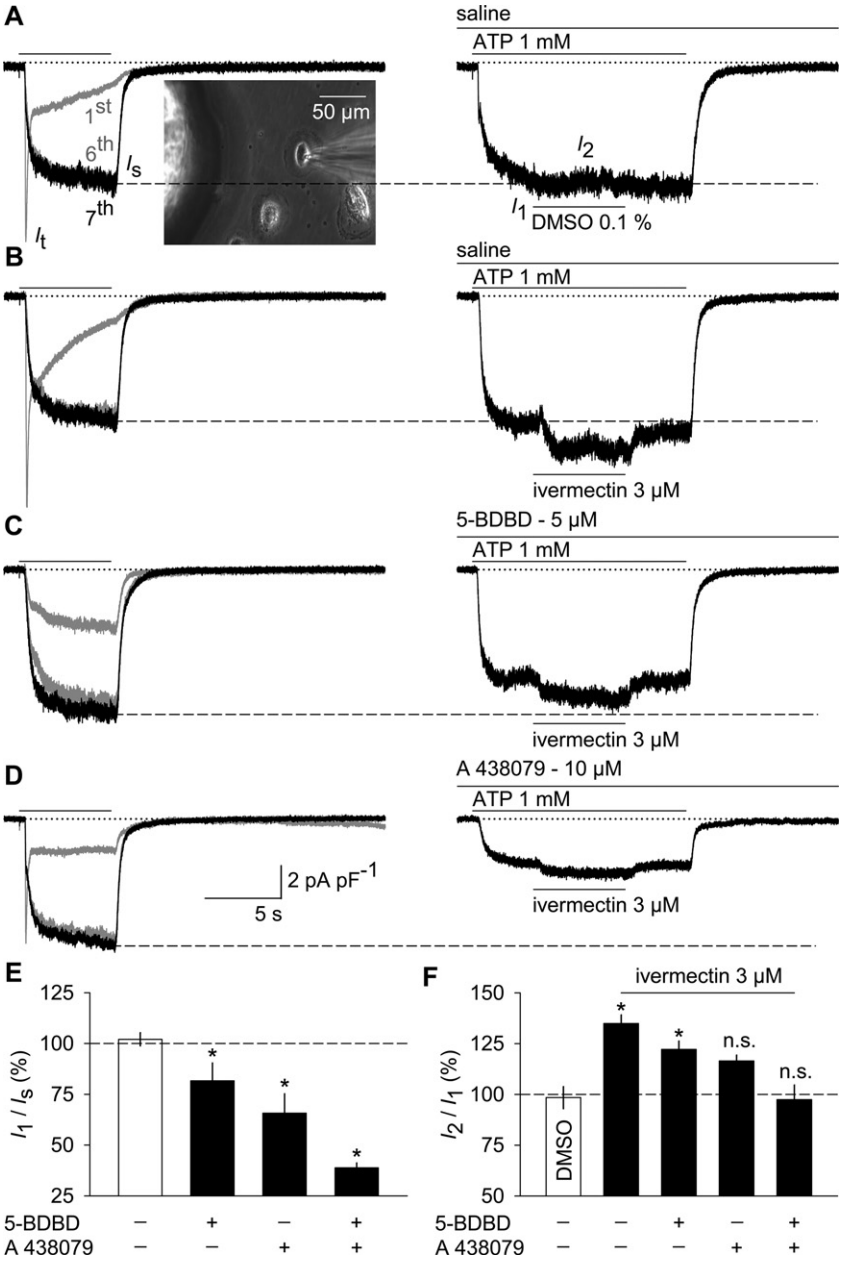

Figure 1

Ivermectin augments sustained ATP-induced currents in hMDM. Human monocytes were obtained from healthy volunteers, and allowed to spontaneously differentiate into hMDM. Whole cell recordings were performed in the voltage-clamp mode at a holding potential of −60 mV and with a bath solution containing low concentrations of divalent cations (low DIC; 0.1 mM $CaCl_2$ and no $MgCl_2$). ATP (1 mM) was applied seven times for 6 s and at 2 min intervals. Shown are superimposed responses to the first, sixth and seventh challenge (left panels in A–D). Note that the first ATP application occasionally elicits a rapidly inactivating current component (transient current, I_t), whereas the following applications cause sustained inward currents (I_s). In panel A–D, dashed lines indicate the levels I_s reached after the run-up of ATP-induced currents (I_{ATP}) was allowed to saturate (usually after five to six ATP pulses). After that, ATP was applied, to the same set of cells, for the eighth time and for 14 s. Solvent (DMSO 0.1 %) or ivermectin (3 µM) was added acutely to ATP for 6 s as indicated by the bars below the current traces in the right panels of A–D. The dotted lines indicate, in this and subsequent electrophysiological figures, the zero current level. The inset in panel A shows a phase contrast microphotograph from the recorded hMDM between the outlet of the perfusion system (left) and the attached patch pipette. Low DIC bath solution (saline; A, B), the P2X4 receptor blocker 5-BDBD (5 µM; C), the P2X7 receptor -specific blocker A 438079 (10 µM; D) or a combination of both (E) were superfused for 4 min before and during the eighth ATP application. (E) Statistical analysis of ATP-induced current densities in $n = 7$–11 experiments performed as illustrated in panels A–D. Columns represent the ratio of I_1 (I_{ATP} just before the application of ivermectin, see panel A) with respect to I_s, expressed as percentage of I_s . *$P < 0.05$, significantly different from the control condition. (F) Statistical analysis of DMSO or ivermectin-induced current potentiation (I_2; peak current in the presence of DMSO or ivermectin, see panel A) without or with pre-incubation of 5-BDBD, A 438079 or 5-BDBD plus A 438079. Columns represent the ratio of I_2 with respect to I_1, expressed as percentage of I_1. *$P < 0.05$, significantly different from the effects of DMSO; n.s., not significant.

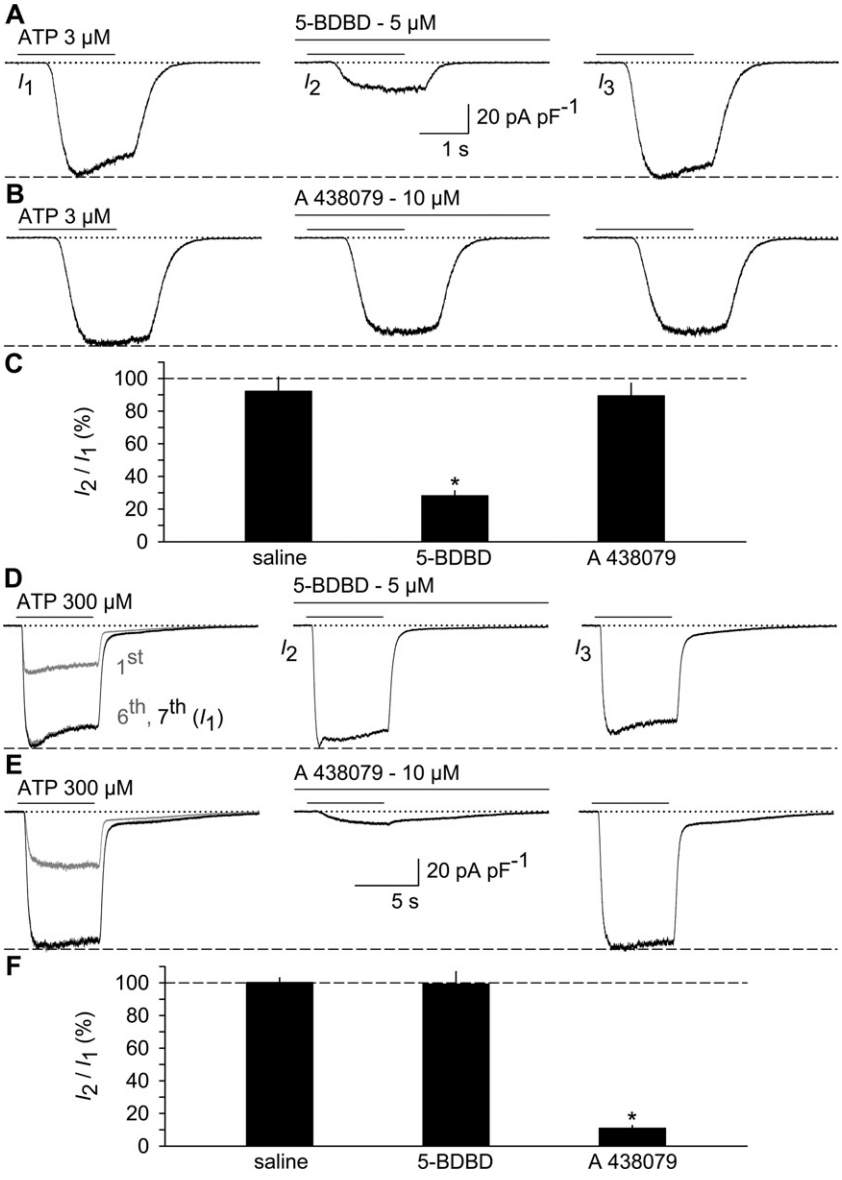

Figure 2

P2X receptor antagonists are differentially effective on recombinantly expressed P2X4 and P2X7 receptors. To confirm the specific activity of receptor blockers, stably transfected HEK cell lines that express human P2X4 receptors (HEK_{hP2X4}; A–C) or human P2X7 receptors (HEK_{hP2X7}; D–F) were stimulated, at a holding potential of −60 mV, with ATP in the absence and in the presence of 5-BDBD (5 μM) or A 438079 (10 μM). A-C), ATP (3 μM) was applied three times (I_1–I_3) for 2 s at 4 min intervals. Low DIC (saline) or low DIC also containing the P2X4 receptor blocker 5-BDBD (A) or the P2X7 receptor blocker A 438079 (B) was superfused 4 min before and during I_2. (C) Statistical analysis of the effects of saline, 5-BDBD and of A 438079 on hP2X4 receptor-mediated currents. The columns represent the ratio of I_2 with respect to I_1, expressed as percentage of I_1. *$P < 0.05$, significantly different from the effects of drug-free low DIC (n = 7–13). Dashed lines in panels A and B indicate the peak current level of the first ATP application (I_1). (D–F) Similar experiments as those in panels A–C, but with a stable HEK_{hP2X7} cell line. Cells were stimulated seven times with 300 μM ATP for 6 s at 2 min intervals to allow run-up of I_{ATP} (superimposed responses to the first, sixth and seventh applications are shown on the left in panels D and E) and then for the eighth (I_2) and ninth time (I_3), but now at 4 min intervals. Low DIC, or low DIC also containing 5-BDBD (D) or A 438079 (E) was superfused for 4 min between the seventh ATP application (I_1) and during I_2 (see panel D). Dashed lines in panels D and E indicate the levels I_{ATP} reached after run-up was allowed to saturate (usually after the fifth or sixth ATP application). (F) Statistical analysis of the effects of 5-BDBD and of A 438079 on hP2X7-mediated currents. *$P < 0.05$, significantly different from the effects of drug-free low DIC (n = 7–19).

divalent concentrations (0.1 mM $CaCl_2$ and no $MgCl_2$; low DIC). Ivermectin enhanced the ATP-triggered inward currents both in the growing phase and under steady-state conditions (i.e. after a run-up of ATP induced current amplitudes had been completed). During the sixth pulse of ATP application, ivermectin potentiated hP2X7 currents by about 1.6- to 1.7-fold compared with the respective time-matching controls and irrespective of the concentration of divalent cations in

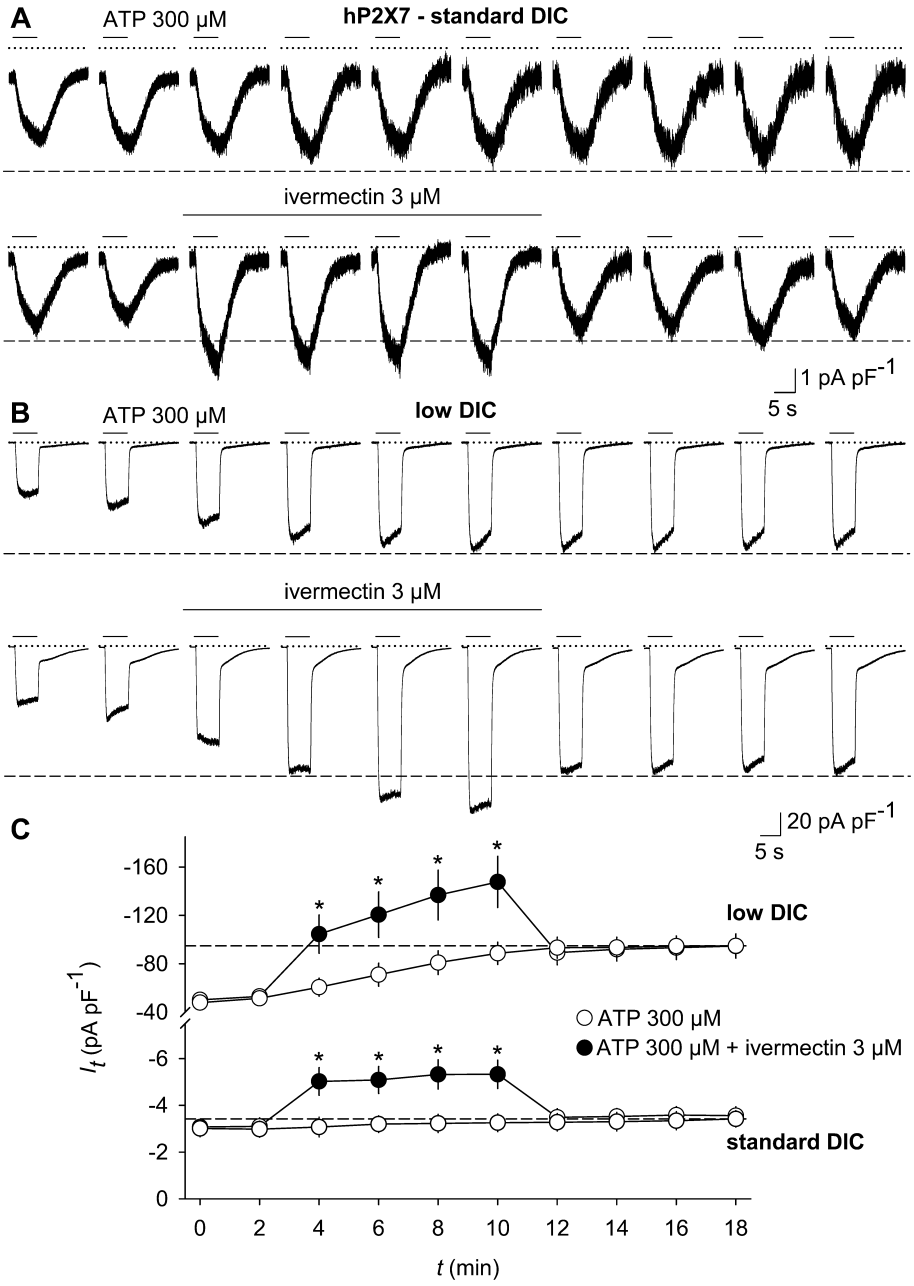

Figure 3

Ivermectin potentiates currents through recombinantly expressed hP2X7 receptors. A stable HEK_{hP2X7} cell line was stimulated, at a holding potential of –60 mV, every 2 min with 10 subsequent applications of 300 µM ATP, applied for 6 s in bath solutions, containing standard (standard DIC, 2 mM $CaCl_2$ and 1 mM $MgCl_2$; A) or low (low DIC, 0.1 mM $CaCl_2$ and no $MgCl_2$; B) concentrations of divalent cations. In some experiments, 3 µM ivermectin was added 2 min before and during the third to sixth pulse of ATP stimulation and then washed out (lower panels in A and B). Dashed lines designate the stage to which ATP-evoked current amplitudes grew in the absence of ivermectin. (C) Statistical analysis of ATP-induced current densities as assessed in panels A and B. Note the different scaling of ATP-triggered current densities assessed in low and standard DIC. *$P < 0.05$, significantly different from current densities in time-matched controls in the absence of ivermectin (n = 12–13).

the bath solution (Figure 3A–C). Hence, ivermectin did not act by overcoming the block of P2X7 receptors that is exerted by extracellular divalent cations (Virginio *et al.*, 1997; Yan *et al.*, 2011) nor did it significantly accelerate the current run-up during repeated ATP application. No change in cell capacitance was detectable during these experiments (e.g. 13.62 ± 0.75, 13.38 ± 0.89 and 13.88 ± 1.08 pF for standard DIC and 12.77 ± 0.78, 12.80 ± 0.88 and 12.41 ± 69 pF for low DIC, before, 6 min, or 12 min after ivermectin application, respectively; P = 0.639; n = 13 each). Therefore, an ivermectin-induced insertion of new P2X7 receptor-bearing vesicles into the plasma membrane appeared to be unlikely.

Concentration-dependence and biophysical properties of ivermectin-potentiated hP2X7 currents

In the HEK_{hP2X7} cell line, ivermectin exhibited a biphasic concentration dependence with a plateau in the range of 0.3–3 μM and an EC_{50} value of the high affinity-binding site of about 56 nM (Hill coefficient nH = 1.5; E_{max} = 134%) and a further rise at ivermectin concentrations >10 μM (Figure 4A,B). Extracellularly applied solvent (0.1% DMSO) or inclusion of 3 μM ivermectin in the pipette solution did not substitute for its addition to the bath solution (Figure 4C). Thus, we suggest that ivermectin binds to the extracellularly accessible part of the channel. Acute application of ivermectin to the ATP-activated channel results in the additional current rapidly developing and reversing (see Figure 4A). A more detailed analysis revealed that a substantial fraction (>93%) of this current increase displayed rise and decay time constants of 200–300 ms, which is in the range of the exchange rate of the perfusion system itself (200–250 ms), indicating a rapid binding and unbinding mode of ivermectin (Figure S2). The ivermectin-induced current augmentation was not associated with shifts of the reversal potentials (–5.9 ± 0.7 and –5.9 ± 0.6 mV in the absence and presence of ivermectin, respectively; n = 10; Figure 4D). Moreover, we could not observe a voltage preference of the potentiating effect (Figure 4D,E), arguing against a putative site of action inside the channel pore or a strong effect on cation selectivity of hP2X7 currents. In the absence of ATP, ivermectin failed to activate hP2X7 currents (Figure S3), thereby ruling out an agonist-like activity of the drug.

Because delayed deactivation kinetics have been demonstrated as a characteristic of ivermectin actions towards P2X4 receptors (Khakh *et al.*, 1999b; Priel and Silberberg, 2004), we tested the inactivation of ATP-triggered hP2X7 currents in the absence and in the presence of 3 μM ivermectin. As described recently (Yan *et al.*, 2010), current decay was best fitted by using the sum of two exponential functions, revealing a fast (τ_1) and a slow time constant (τ_2; see right panels in Figure 5A,B). Whereas τ_2 contributed 18–23% of the amplitude and showed little change over time (D in Figure 5), the major fraction of the amplitude decayed with a fast time constant τ_1 that was growing during repetitive ATP application (Figure 5C,D). Despite inducing a current potentiation, ivermectin had no discernible effect on either time constant. We conclude that ivermectin is a rapidly binding and unbinding allosteric modulator of ATP-stimulated hP2X7 receptors.

Up to now, the positive modulation of hP2X7 receptors by ivermectin appeared similar to the effects of other positive P2X7 receptor modulators, including polymyxin B (Ferrari *et al.*, 2007), arachidonic acid (Alloisio *et al.*, 2006) or clemastine (Nörenberg *et al.*, 2011). These modulators share the property of sensitizing P2X7 receptors to lower ATP concentrations without changing the maximum obtainable effects in the presence of saturating ATP concentrations. When testing ivermectin on hP2X7 currents induced by increasing ATP concentrations, however, the mode of action revealed an increase in current amplitudes at all ATP concentrations tested, including the saturating concentration of 10 mM ATP (Figure 6A,B). The EC_{50} of ATP shifted only slightly from 355 ± 31 to 274 ± 20 μM (P = 0.037) after pre-incubation with ivermectin. The slight and statistically non-significant (P = 0.094) rise of Hill coefficients from 1.75 ± 0.05 with ATP alone to 1.92 ± 0.1 in the presence of ivermectin indicated only a minor effect of ivermectin on the cooperativity of ATP binding (n = 14 each; Figure 6C,D). The respective maximal current densities of –349 ± 30 and –447 ± 19 $pA{\cdot}pF^{-1}$ in the absence and presence of 3 μM ivermectin were significantly different (P = 0.003) and were achieved at 10 mM ATP, a concentration that was maximally effective under low DIC conditions. As concentration–response curves with and without ivermectin were obtained in different cells, the increase in maximum current was confirmed by challenging the same cell with 0.3 and 10 mM ATP, and adding ivermectin. The data confirmed the reversible potentiation of hP2X7 currents that are elicited by either non-saturating or saturating ATP concentrations (see also Figure S4).

Ivermectin potentiates Ca^{2+} signalling, but not Yo-Pro-1 and $NMDG^+$ influx through hP2X7 receptors

In fluorimetric $[Ca^{2+}]_i$ assays, the potentiating effect of ivermectin on ATP-triggered Ca^{2+} entry through stably expressed human P2X7 receptors was reproduced (Figure 7A). Again, submicromolar ivermectin concentrations elicited a potentiation of the intracellular steady-state Ca^{2+} concentrations by about 15%, which was further enhanced at ivermectin concentrations of 10–50 μM and abolished by the ATP-competitive P2X7 receptor blocker A 438079 (10 μM; see Figure 7A,B) or of the highly potent non-competitive P2X7 receptor blocker AZ 10606120 (1 μM; data not shown).

Interestingly and in contrast to what has been observed with the positive P2X7 receptor modulator clemastine, the ATP-induced and A 438079-sensitive entry of the large cationic dye Yo-Pro-1 was not accelerated in the presence of 30 μM ivermectin (Figure 7C,D). Likewise, the dilation of the hP2X7 pore appeared unaffected by ivermectin. First, we assessed the current kinetics at a holding potential V_H = –60 mV during replacement of extracellular metal cations by the large organic cation $NMDG^+$. Under these conditions, ATP stimulation gives rise to outward currents carried by Na^+ in the pipette solution, followed by current reversal and development of a $NMDG^+$-carried inward current (Figure 8A,B). The peak amplitudes of the initial Na^+ outward current and the late $NMDG^+$ inward current were 25.4 ± 2.7 and 22.3 ± 4.7 $pA{\cdot}pF^{-1}$ (P = 0.271) and –25.8 ± 3.5 and –23.9 ± 3.5 $pA{\cdot}pF^{-1}$ (P = 0.826; n = 13 and 12) in the absence and presence of ivermectin, respectively. Next we investigated the time-dependent shift of reversal potentials (V_{revs}) to more positive potentials in $NMDG^+$-containing bath solutions, indicating a progressive increase in the permeability ratio for $NMDG^+$ with respect to Na^+ (P_{NMDG}/P_{Na}). Here, the V_{rev} shifted from –65.2 ± 0.7 and –63.7 ± 0.8 mV (P = 0.158) to steady-state values of –44.8 ± 3.2 and –45.7 ± 2.2 mV (P = 0.757; n = 9 each) in the absence and presence of ivermectin respectively (Figure 8C–E). When calculated from the experimentally observed V_{rev} values, P_{NMDG}/P_{Na} changed from 0.073 ± 0.002 (controls) and 0.078 ± 0.002 (ivermectin-treated cells; P = 0.158) at 4 s after the stimulation with ATP to 0.177 ± 0.027 and 0.163 ± 0.014 in the continued (90 s) presence of ATP. When comparing the permeability ratios in the absence

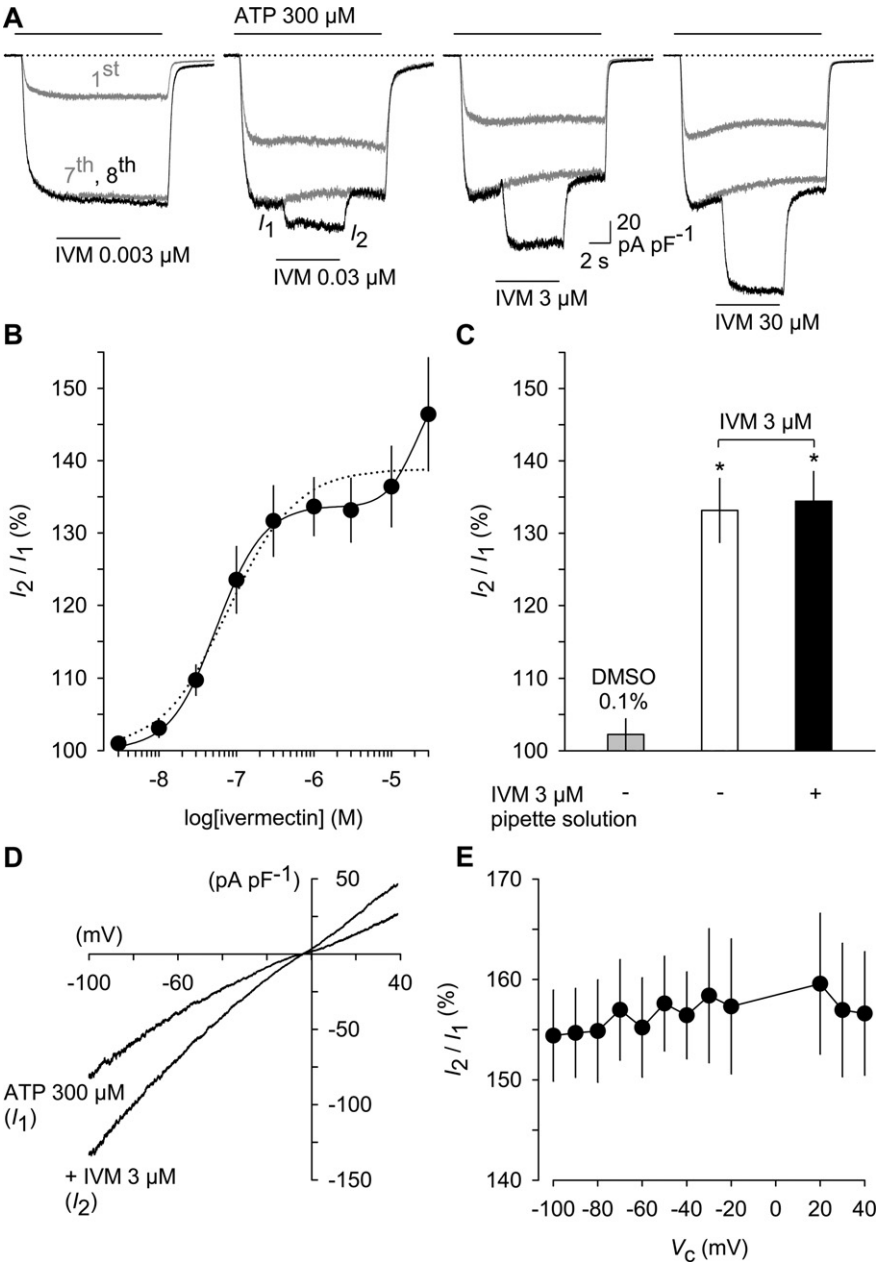

Figure 4

Characterization of ivermectin effects on recombinant hP2X7 receptors. (A,B) Concentration–response curves of ivermectin (IVM)-induced hP2X7 current potentiation were recorded in low DIC bath solution and at a holding potential of −60 mV by applying repetitive pulses of ATP stimulation (300 μM for 14 s every 2 min for seven times) to allow for run-up of I_{ATP} and then acutely adding, for 6 s, various concentrations of ivermectin, 4 s after an eighth application of ATP was initiated. Representative responses to the first and seventh ATP application and the eighth ATP/ivermectin co-application are shown superimposed in panel A. (B) Statistical analysis of experiments performed as shown in panel A with superposed mathematical fit according to one or two affinity states of ivermectin. Each data point represents the ratio of the ivermectin-augmented current (I_2) with respect to the current immediately before application of ivermectin (I_1, see panel A), expressed as percentage of I_1 as derived from n = 7–10 independent measurements. (C) Inclusion of 3 μM ivermectin (IVM) in the pipette solution does not prevent or attenuate ivermectin potentiation applied via the bath solution. Shown is the statistical analysis of similar experiments as those in panel A. HEK_{hP2X7} cells were alternately microdialysed with either standard pipette solution (n = 8) or with standard pipette solution containing 3 μM ivermectin (n = 7). Note that acute extracellular application of the solvent (DMSO 0.1%) does not substitute for the potentiating effect of ivermectin (n = 10). *P < 0.05, significant differences from the effects of 0.1% DMSO. (D) Current–voltage relationship of ATP-triggered and ivermectin-augmented hP2X7 currents were tested by applying slow voltage ramps. Voltage ramps, extending from −100 to 40 mV, were 1 s in duration and imposed every 2 s on a holding potential of −60 mV. Illustrated are representative leak-subtracted *IV* traces for the ATP (300 μM)-induced current in the absence (I_1) and presence of ivermectin (3 μM; I_2). Leak subtraction was done by subtracting the ensemble current from 4 V ramps recorded prior to ATP application from that obtained after 4 s in the presence of ATP and that after another 4 s in the additional presence of ivermectin. (E) Ratios of ivermectin-potentiated (I_2) and non-potentiated ATP currents (I_1) are calculated at different command potentials (V_C).

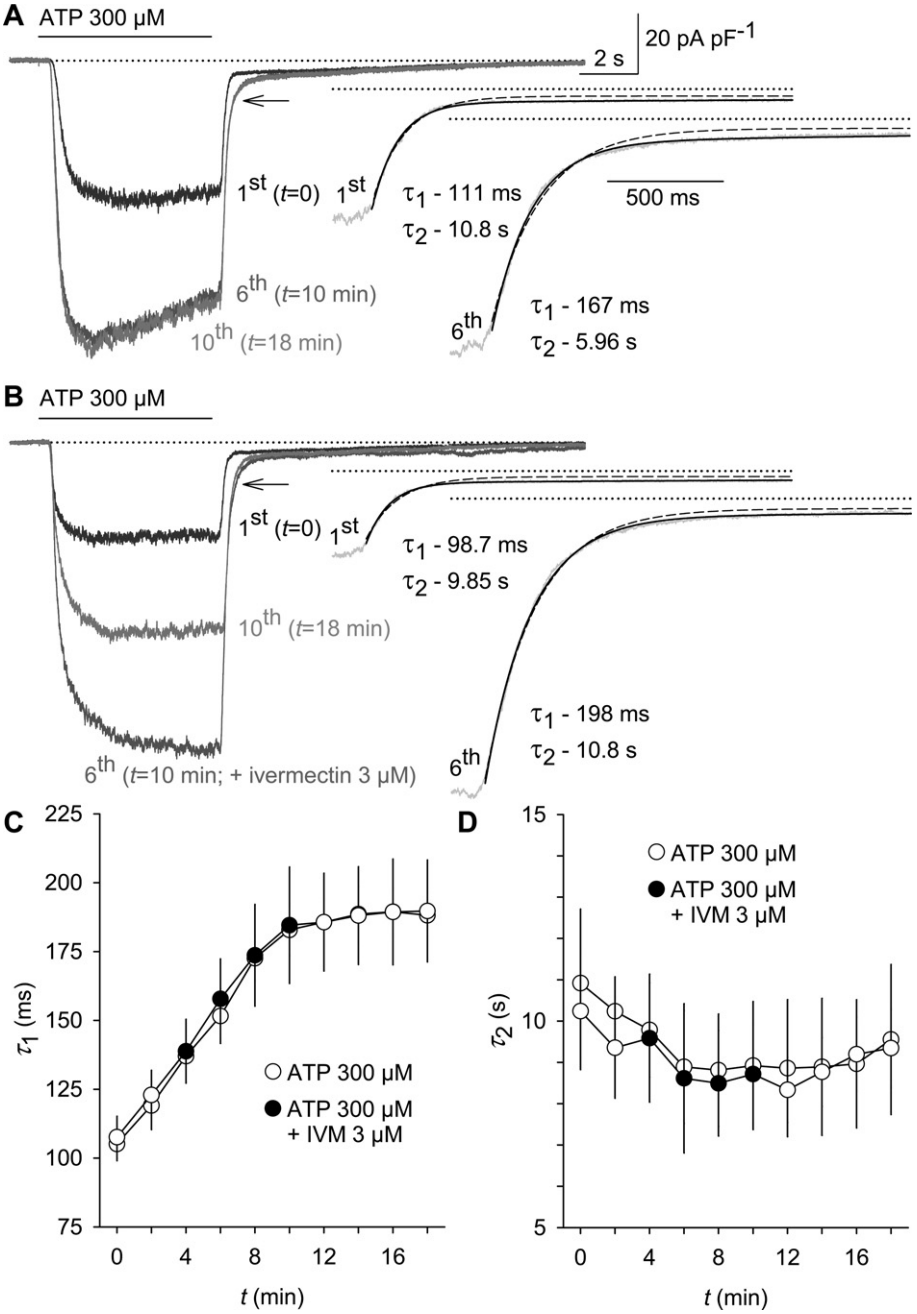

Figure 5

Current decay after ATP removal is delayed upon repetitive hP2X7 receptor stimulation, but not additionally delayed by ivermectin. ATP (300 μM) was applied to voltage-clamped (−60 mV) HEK_{hP2X7} cells 10 times for 6 s at 2 min intervals in low DIC. (A) The left panel depicts a superposition of the first, 6th and 10th pulse of ATP stimulation. Note the broadening of current amplitudes during repetitive stimulation (arrow). Right: monoexponential and bi-exponential fits of the current decay are superimposed, and the corresponding values for fast (τ_1) and slow (τ_2) time constants are depicted. Dotted lines: zero current level. (B) 3 μM ivermectin was added to the bath solution during the third to sixth pulse of ATP stimulation. (C,D) Statistical analysis of 12 independent experiments, each performed in the absence or in the presence of 3 μM ivermectin (IVM) as shown in panels A and B.

or presence of ivermectin, no significant differences were discernible. Similarly, the time constants of time-dependent shifts of the reversal potentials did not differ significantly between ivermectin-treated cells (23.7 s) and the solvent controls (21.8 s). We conclude that ivermectin potentiates ionic currents through hP2X7 receptors without changing the intrinsic property of the hP2X7 pore to dilate and become permeable for large organic cations.

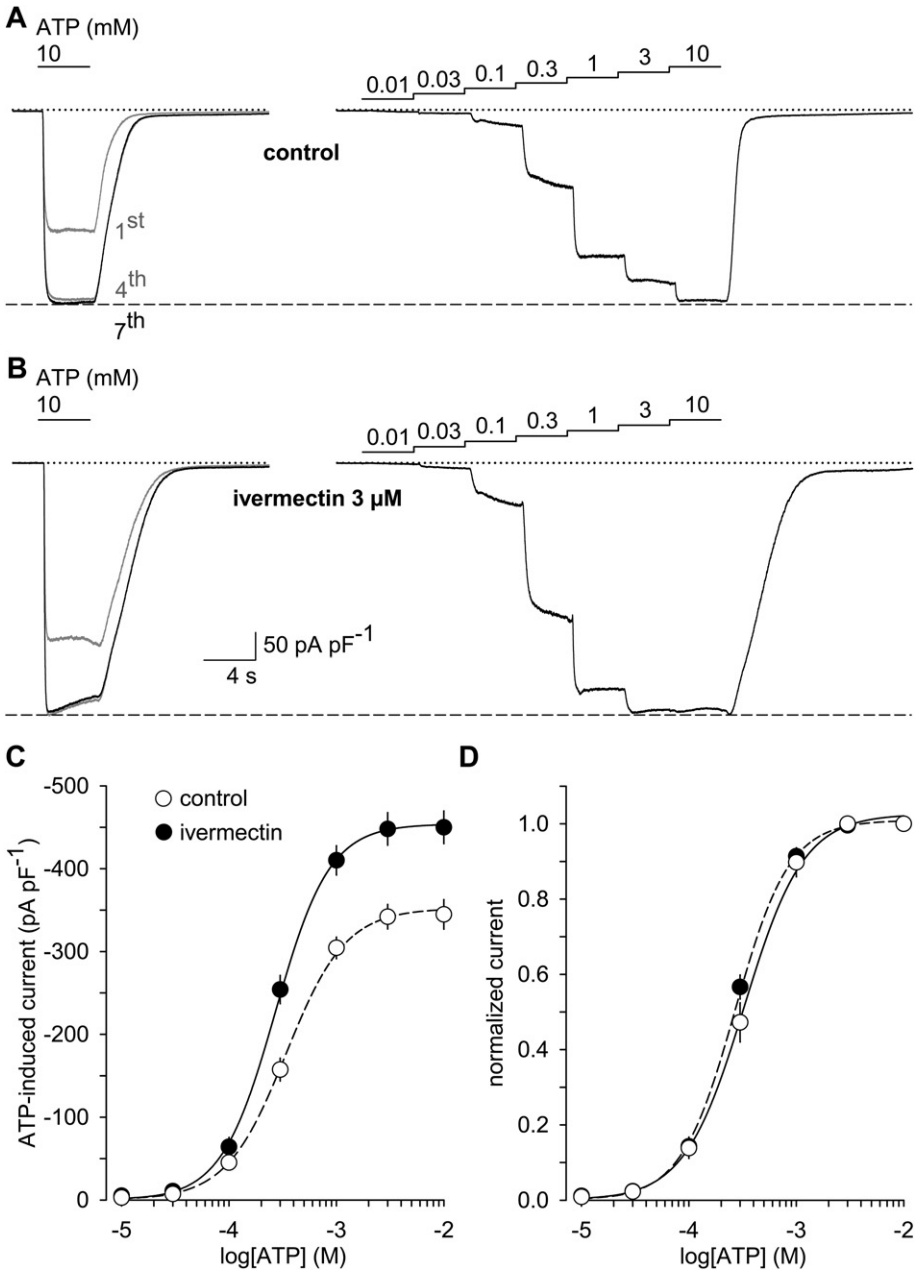

Figure 6

Ivermectin augments ATP-induced hP2X7 currents without strongly affecting the ATP sensitivity. (A and B) Voltage-clamped (−60 mV) HEK_{hP2X7} cells were repetitively stimulated for 4 s with 10 mM ATP in low DIC and at 2 min intervals until the hP2X7 current run-up was completed in the seventh pulse (left panels) and then subjected to a stepwise increase in ATP concentrations (right panels; each step 4 s in duration). Dashed lines indicate the levels I_{ATP} reached after run-up was allowed to saturate. In experiments with ivermectin (3 µM; B), the modulator was present for at least 10 min before the trials were initiated and throughout their time course. (C, D) Data of $n = 14$ experiments performed as shown in panels A and B were accumulated to obtain absolute (C) and normalized (with respect to the effects of 10 mM ATP; D) concentration–response functions of ATP in the absence and in the presence of ivermectin. Note the minor effect of ivermectin on the EC_{50} value and on the slope (Hill coefficient) of the ATP concentration–response relationship (D).

Ivermectin is only poorly effective at mouse and rat P2X7 receptors

Our data are in conflict with the recent assumption that ivermectin potentiation would be P2X4 receptor-specific, raising the question why its modulatory effect on P2X7 receptors had been overlooked. Because the original specificity tests were conducted in *Xenopus laevis* oocytes after injection of a rat P2X7 receptor cRNA construct (B. Khakh, personal communication), we reassessed the effects of ivermectin in primary cultures of rat and mouse cortical astrocytes that endogenously express P2X7 receptors (Duan *et al.*,

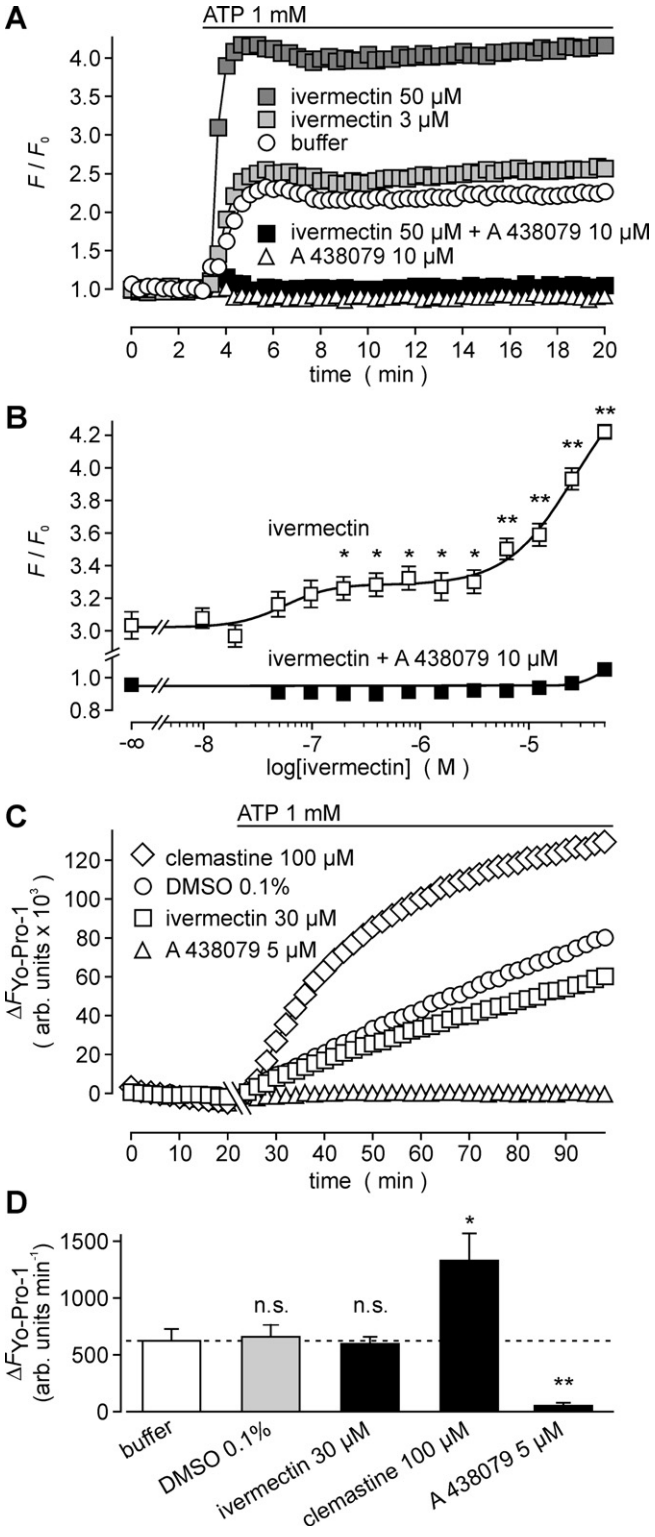

Figure 7

Ivermectin potentiates $[Ca^{2+}]_i$ signals but not Yo-Pro-1 entry in HEK_{hP2X7} cells. (A) Fluo-4-loaded HEK_{hP2X7} cell suspensions were subjected to fluorimetric $[Ca^{2+}]_i$ analysis in a fluorescence plate imager. Cell suspensions were pretreated for 5 min with the indicated modulators, their maximal solvent concentration (0.1% DMSO) or buffer as indicated, and stimulated with 1 mM ATP. Background-corrected signal F values were normalized to their respective initial intensities F_0. (B) Experiments with various ivermectin concentrations were performed as shown in panel A. Means ± SEM of 36 dilution series measured in five independent experiments are shown. Note the discontinuous scale of the axes. $^*P < 0.05$; $^{**}P < 0.01$, significantly different from corresponding solvent controls. (C) HEK_{hP2X7} cell suspensions were re-suspended in HBS, containing 0.1 mM $CaCl_2$ and no $MgCl_2$ (low-DIC HBS), and 2 µM Yo-Pro-1. The indicated modulators were added 5 min prior to the measurement. Fluorescence signals were recorded in a plate reader before and after injection of 1 mM ATP (final concentration). (D) Statistical analysis of experiments performed as shown in panel C. Means and SE of n = 4–6 independent experiments performed in duplicates are shown.

2003; Nörenberg *et al.*, 2010) as well as in recombinantly rat P2X7 receptor-expressing HEK293 cells. Clemastine, but not ivermectin, induced a reversible current potentiation in these rodent astroglia cultures, when grown in standard culturing conditions. When maintained in serum-free culture media that contain a G5 supplement, astrocytes showed a stellate shape with elongated processes, reminiscent of an activated phenotype (Figure 9A,B). Immunofluorescence analysis had previously revealed an up-regulation of P2X7 protein expression, e.g. in rat cortical astrocytes *in situ*, that were activated by middle cerebral artery occlusion in a focal cerebral ischaemia model (Franke *et al.*, 2004). Consistently, current densities were 1.5- and 3.3-fold higher in G5-treated mouse and rat astrocytes, respectively, compared with cultures grown in standard media. In these cells, P2X7 currents elicited by 0.3 mM ATP were again unaffected by ivermectin, whereas the potentiating effect of clemastine was robustly reproduced (Figure 9A–C). In mouse astroglial cultures, the findings were essentially identical to those observed in rat astrocyte cultures (Figure 9C). In the presence of the P2X7 receptor blocker A 438079, the ATP-triggered currents were strongly suppressed in all types of astroglia used, while 5-BDBD had no discernible effect (Figure 9D–F). In G5 supplement-treated and fluo-4-loaded rat astroglia cell suspensions, BzATP (100 µM) elicited A 438079-sensitive increases in $[Ca^{2+}]_i$, which were strongly potentiated by clemastine (Figure S5A,B). At concentrations up to 10 µM, ivermectin treatment failed to enhance the BzATP-induced, P2X7-like Ca^{2+} signals in G5-treated rat astroglia (Figure S5C,D). A slight potentiation was discernible only at ivermectin concentrations of 20–50 µM that are not commonly applied when using this drug for selectivity tests. Ivermectin also failed to potentiate ATP-induced currents in HEK293 cells stably expressing rat P2X7 receptors (Figure S6), excluding the possibility that its inability to modulate rat P2X7 receptors was limited to the astroglial cell model. These observations confirm the notion that P2X7 receptors are the most prominent molecular substrate of the sustained currents in the murine astrocyte culture model and corroborate the finding that the potent ivermectin-induced augmentation of P2X7 receptor activity is a species-specific phenomenon that is lacking in the murine orthologues.

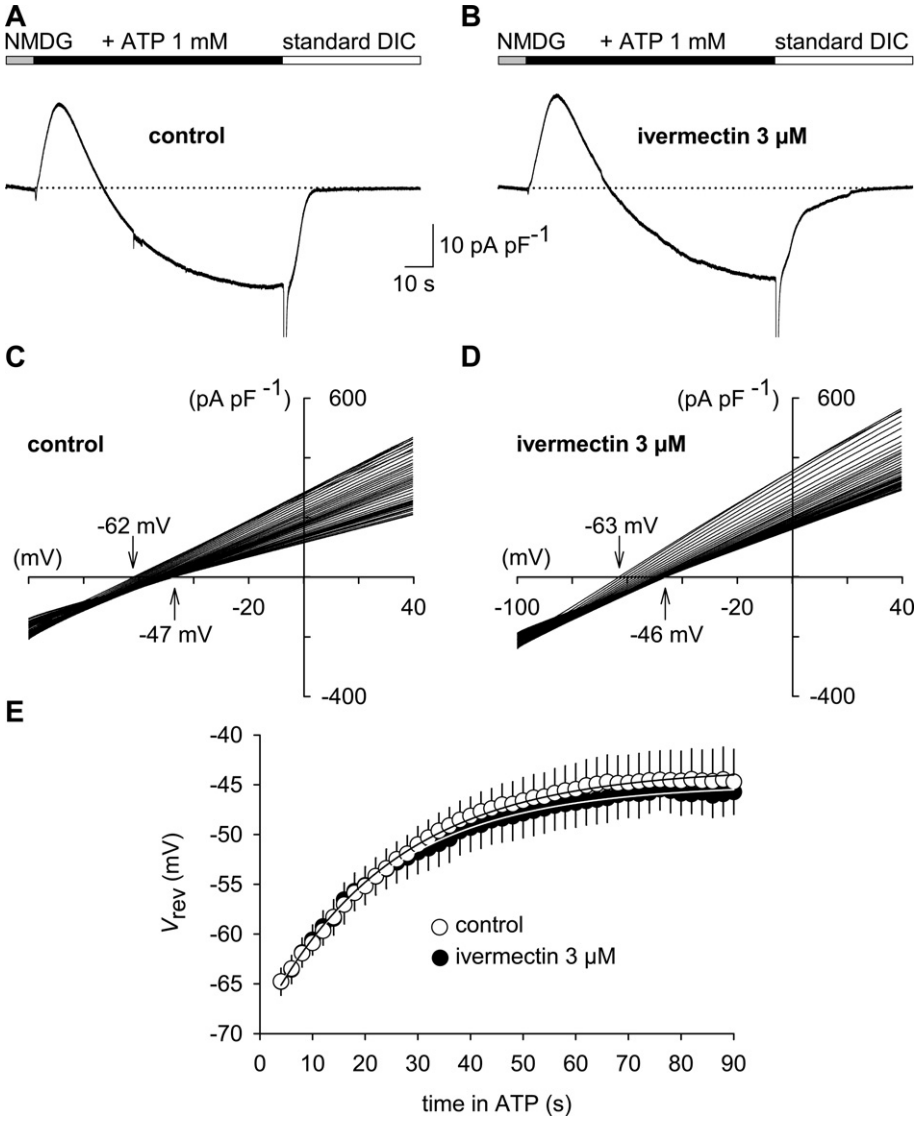

Figure 8

Ivermectin does not accelerate the ATP-induced pore dilation as monitored by $NMDG^+$ permeation properties. (A and B) Voltage-clamped (−60 mV) HEK_{hP2X7} cells were stimulated for 90 s with 1 mM ATP in a bath solution, containing $NMDG^+$ as the only positive charge carrier. Note that an initial outward current carried by Na^+ (the only cation in the pipette solution) is transiently detectable, followed by a slower decay, current reversal and a sustained development of inward currents (carried by $NMDG^+$) both in the absence (A) or presence (B) of 3 µM ivermectin. The large tail currents (only partially shown) observed on terminating the stimulation with ATP and switching to a NaCl-based standard DIC solution indicate a Na^+ permeability preceding the hP2X7 channel closure. The current traces shown in panels A and B are representative for 12 and 13 similar experiments conducted in the absence and presence of ivermectin respectively. In a ramp protocol (ramps of 1 s in duration, extending from −100 to +40 mV and evoked at 2 s intervals), imposed under otherwise the same experimental conditions as used in panels A and B, continuous stimulation with ATP leads to a time-dependent shift of reversal potentials to more positive values (see arrows) irrespective of the absence (C) or presence (D) of 3 µM ivermectin. Note the parallel decrease in ramp current slope, also suggesting that $NMDG^+$ only partially substitutes for Na^+ as the conducted ion. Superimposed current traces shown are leak-corrected by subtracting the ensemble current from 4 V ramps recorded prior to ATP application. (E) Reversal potentials were calculated from $n = 9$ data sets each, obtained as shown in panel C or D, and depicted versus time in ATP. To obtain the pore dilation time constants, data were fitted to a monoexponential growth to maximum function by nonlinear regression analysis.

Discussion

In this paper we provide evidence for a potent ivermectin-induced augmentation of ATP-induced currents and $[Ca^{2+}]_i$ signals through recombinantly or natively expressed human P2X7 receptors. Ivermectin can therefore no longer be considered a P2X4 receptor-specific tool in human tissues. Allosteric positive modulation of hP2X7 receptors by ivermectin is effective at saturating or submaximally effective ATP concentrations and may mislead the investigator to assume an involvement of P2X4 receptors. Our results further confirm the initial data that ivermectin has little effect on mouse or

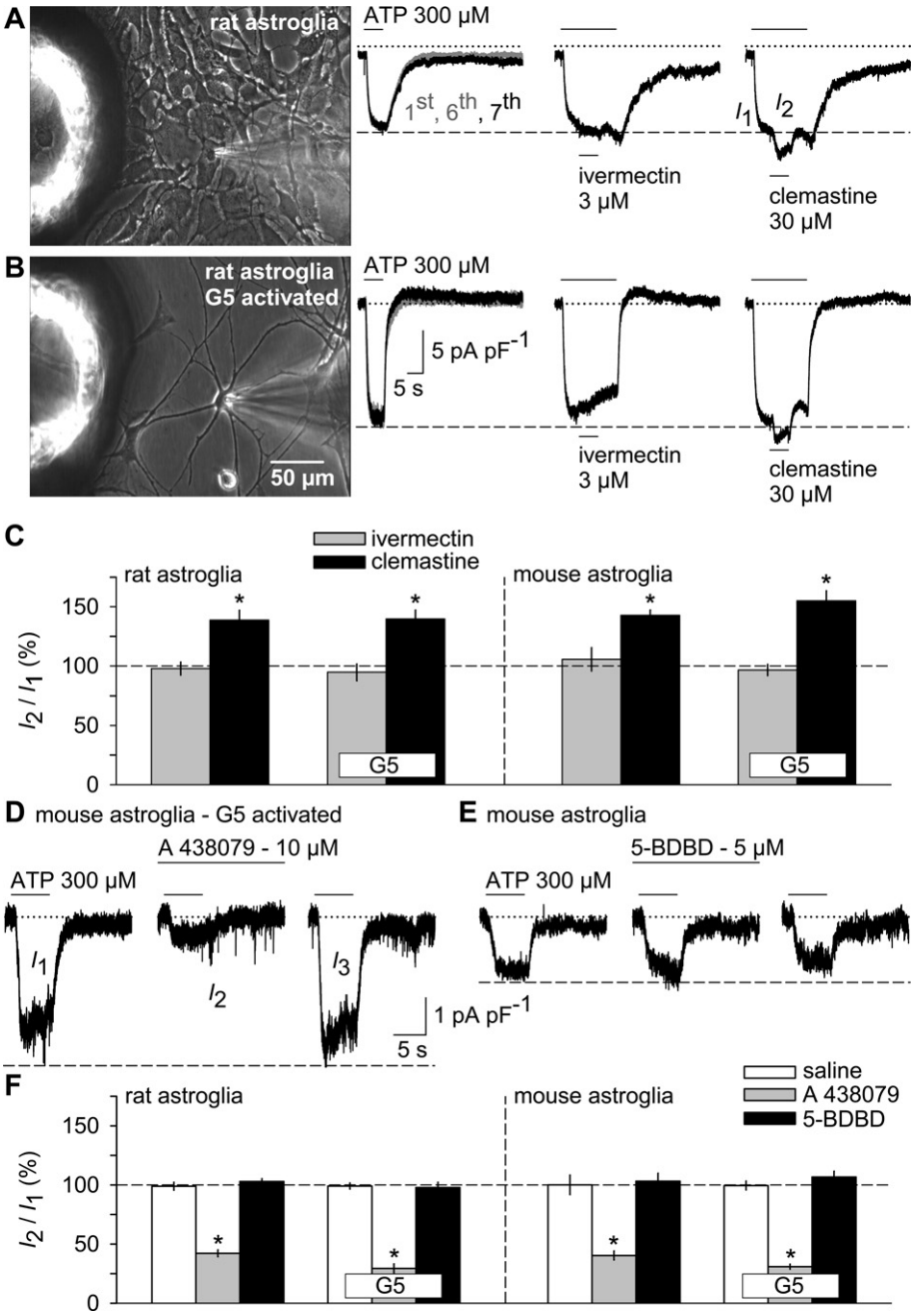

Figure 9

Ivermectin is ineffective at murine P2X7 receptors in astroglia cultures. Rat astroglia cultures were obtained and maintained either in standard culturing conditions (A) or in G5 supplement-containing activation medium (B). Note the elongated processes in panel B that correspond to a phenotypic modulation reminiscent of activated, stellate forms of astroglia. During repetitive pulses of ATP stimulation (300 μM), at a holding potential of –80 mV and in low DIC bath solution, supplemented with the gap junction blocker carbenoxolone (100 μM), ivermectin (3 μM) or clemastine (30 μM) were added to the bath solution as indicated. Note the lack of current run-up during repetitive stimulation with ATP. Superimposed responses to the first, sixth and seventh challenge with ATP are shown at the left in panels A and B. (C) Current densities before (I_1) and after addition of the respective modulator (I_2) were quantified to calculate means and SE in quiescent or G5-activated forms of rat astrocytes (left). Similar experiments were repeated with mouse astrocytes (right). * $P < 0.05$, significantly different from the effect of ivermectin ($n = 10$ each). Effects of the P2X7 blocker A 438079 (10 μM; D) and the P2X4 blocker 5-BDPD (5 μM; E) on ATP-induced currents in mouse astroglial cells grown either under standard conditions (E) or in the presence of G5 (D). Cells were stimulated three times (I_1 to I_3) with ATP for 6 s and at 4 min intervals. Low DIC (saline) or low DIC containing A 438079 or 5-BDBD was superfused 4 min before and during I_2. (F) Summary of experiments performed as in panels D and E on rat (left) or mouse (right) astroglial cells. * $P < 0.05$, significantly different from the corresponding saline control values ($n = 6–8$).

rat P2X7 receptors. A species-specific allosteric modulation of P2X7 receptors has been observed with a number of compounds (Michel *et al.*, 2009; Coddou *et al.*, 2011). Thus, species-related differences have to be taken into account when relying on small molecules for probing native P2X4 and P2X7 channels. Despite its reliability in rat and mouse tissues, findings that are based on the application of ivermectin in cells and tissues obtained from humans or possibly other higher mammals, need critical re-evaluation.

Because of the involvement of P2X7 receptors in inflammation and pain generation (Donnelly-Roberts *et al.*, 2008), highly specific and potent blockers of these receptors have been developed, and clinical trials are either underway or completed (Lenertz *et al.*, 2011). In contrast, P2X4 receptor-specific tools are still underrepresented, and experiences with the recently disclosed P2X4 receptor blocker 5-BDBD (Donnelly-Roberts *et al.*, 2008) are limited. Moreover, 5-BDBD has only a modest potency to block recombinant hP2X4 (see Figure 2) or native P2X4-like receptors in vascular endothelial cells from guinea pig cochlea (IC_{50} ~ 30 μM; Wu *et al.*, 2011). Nonetheless, 5-BDBD is currently the only useful compound to probe human P2X4 channels directly. Hence, a pharmacological hP2X4 receptor identification should be complemented, for example by biophysical profiling, ATP sensitivity tests, assessing the Zn^{2+} sensitivity (Wildman *et al.*, 1999; Coddou *et al.*, 2007) or, ideally, by knock-down approaches.

As the mode of action of ivermectin potentiation of P2X4 receptors includes a delayed inactivation upon ATP removal (Khakh *et al.*, 1999b; Priel and Silberberg, 2004), whereas hP2X7 receptors do not show this phenomenon (present study), ivermectin may remain a valuable tool in electrophysiological assays applied to human tissues in combination with appropriate analyses of current decay behaviour.

Ivermectin, having a greater molecular diameter of about 21 Å (Jelínkova *et al.*, 2008), is thought to bind to P2X4 receptors within the upper half of TM1 and TM2 (Silberberg *et al.*, 2007; Jelínkova *et al.*, 2008). Despite potentiation of ATP-induced currents through hP2X7 receptors, ivermectin scarcely interfered with ATP sensitivity and the delay of current decay upon ATP wash-out. These properties are in contrast to those seen in P2X4 receptors, but reminiscent of ivermectin effects on ancestral P2X receptors in the trematode *Schistosoma mansoni* or in the water bear *Hypsibius dujardini* (Agboh *et al.*, 2004; Bavan *et al.*, 2009), which carry a single P2X receptor gene. Since the seven mammalian P2X receptor genes have divided at a much later stage during evolution, none of them can be considered as direct ortholog of these ancestral members. Since ivermectin is not an endogenous compound, there is probably no phylogenetic pressure to maintain the biological effect of this modulator during evolution and amongst various mammalian species. Hence, the existence of similar effects of ivermectin on P2X receptors in highly diverse classes such as Eutardigrada and Mammalia is an intriguing fact.

Recent work describing fundamental events of P2X4 receptor gating by probing the channel's transmembrane segment rotation with ivermectin (Silberberg *et al.*, 2007) may provide a clue to this puzzling question, since rotational transmembrane helix mobility that underlies the channel gating may have contributed to co-conserve an ivermectin-binding helix interface, despite the variable impact on distinct mammalian P2X receptor isoforms and orthologues. This view may be fostered by the fact that ivermectin also acts as a positive allosteric modulator of genetically unrelated vertebrate Cys-loop receptors such as the α7 nicotinic acetylcholine receptors (Collins and Millar, 2010), $GABA_A$ receptors (Dawson *et al.*, 2000), glycine receptors (Dawson *et al.*, 2000; Lynagh *et al.*, 2011), or the nematode glutamate-gated chloride channel, GluCl (Hibbs and Gouaux, 2011).

In order to identify possible ivermectin binding sites at hP2X7 receptors, we aligned the respective amino acid sequences of this receptor with the corresponding portions of other ivermectin-sensitive P2X receptors (rat and human P2X4, *S. mansoni* P2X, *H. dujardini* P2X) and compared them with the poorly sensitive mouse and rat P2X7 receptors. However, we and others (Silberberg *et al.*, 2007; Jelínkova *et al.*, 2008) were unable to delineate a conserved ivermectin-binding motif. It has, therefore, been suggested for P2X4 receptors that the main determinant of ivermectin binding is the shape of the hydrophobic crevice, which is formed at the lipid–protein interface by an outward rotation of the TMs during gating, and thereby hinders a back-rotation of TM1 and channel closure (Silberberg *et al.*, 2007). This view is also consistent with the recently solved crystal structure of the *Caenorhabditis elegans* GluCl. Here, the lactone moiety intercalates between the transmembrane-spanning helices TM1 and TM3, locally distorts the structure, allowing access to the pore-aligning TM2 and stabilizes it in the open pore conformation (Hibbs and Gouaux, 2011). Moreover, mutagenesis data obtained with the human α1 glycine receptor corroborate the insertion of ivermectin between TM helices (Lynagh *et al.*, 2011). As to the nicotinic and glycine receptors, the situation may be similar. Here, ivermectin apparently binds between TM1 and TM4 of the nicotinic receptor α7 subunit (Collins and Millar, 2010) or between TM2 and TM3 of the glycine receptor α1 subunit (Lynagh *et al.*, 2011) to exert its modulatory effects. Beyond that, intercalation between TM segments may constitute a more general mechanism for positive allostery at ligand-gated ion channels that is shared by a variety of chemically diverse modulators of, for example $GABA_A$ and glycine receptors, such as neurosteroids, volatile anaesthetics and ethanol (Mihic *et al.*, 1997; Ye *et al.*, 1998; Hosie *et al.*, 2006).

In case of the above-mentioned members of the Cys-loop family of ligand-gated channels, it is thought that the allosteric compounds most likely gain access to their site of action via a water-accessible intrasubunit cavity, extending from the extracellular side of the transmembrane helices about halfway down into the lipid bilayer (Mihic *et al.*, 1997; Ye *et al.*, 1998; Hosie *et al.*, 2006; Collins and Millar, 2010; but see Lynagh *et al.*, 2011). Because ivermectin was only active at hP2X7 (present study) or at hP2X4 receptors (Priel and Silberberg, 2004), when applied from the extracellular side of the cell membrane, a similar access path for the compound may be assumed also for hP2X7 receptors. The crystallographic analysis of P2X4 receptors offers no obvious hints for the existence of an aqueous access path in the closed conformation of the channel (Kawate *et al.*, 2009). However, the highly lipophilic ivermectin molecule (log*P* = 4.8) may reach its hypothetical site of attack, a hydrophobic crevice between TM1 and TM2 that may be opened during channel activation by an outward rotation of TM1, by partitioning into the lipid

membrane (Silberberg *et al.*, 2007). Considering that a Bodipy-labelled ivermectin has been shown to partition into the outer leaflet of plasma membranes, but not to cross the whole lipid bilayer (Martin and Kusel, 1992), the difference in effects between extracellular and intracellular application of the drug may result from its physicochemical properties.

Intriguingly, despite potentiation of current amplitudes at all ATP concentrations, the development of $NMDG^+$ permeability and Yo-Pro-1 uptake were not affected by ivermectin. The mechanisms underlying the pore dilation are still not fully understood. One of the biophysical correlates of on-going receptor sensitization, coincident with an increased $NMDG^+$ permeability, is a progressive delay in current decay after ATP wash-out (Yan *et al.*, 2010). Ivermectin did not interfere with P2X7 current decay nor did it substantially increase ATP cooperativity. Its mode of action did, hence, clearly not involve the promotion of receptor sensitization (pore dilation), explaining the lack of effect on $NMDG^+$ permeability. Besides of changing the affinity of the receptors for ATP, allosteric modulators may also strengthen the transduction of signals from the agonist binding site to the receptor gate (Yan *et al.*, 2010). Thus, we propose that, similar to the situation described for P2X4 receptors (Silberberg *et al.*, 2007), ivermectin may hinder the closure of the hP2X7 pore. The resulting increase in open probability would than explain the potentiation of ATP-responses without any additional need for an increase in P2X7 receptor conductance (i.e. sensitization or pore dilation). Hence, the mode of action of ivermectin and that of clemastine, arachidonic acid and polymyxin B appear to differ profoundly (Alloisio *et al.*, 2006; Ferrari *et al.*, 2007; Nörenberg *et al.*, 2011).

Based on published data, we expected that both hMDM and murine astrocytes would express considerable amounts of P2X4 receptors (Guo *et al.*, 2007; Fischer *et al.*, 2009; but see Lalo *et al.*, 2008). Whilst leaving this possibility open, data obtained with receptor blockers point to a prominent role of P2X7 receptors in mediating non-inactivating currents in these cell models at least when cultured for 4–14 days. It should be mentioned that P2X7 receptors are also the predominant functional P2X receptor found in murine astrocytes *in situ* in the prefrontal cortex and in hippocampal slices (Fellin *et al.*, 2006; Oliveira *et al.*, 2011). The fact that P2X7 receptors are functionally up-regulated in certain culturing conditions is well substantiated by the observation that ATP-triggered and A 438079-sensitive sustained currents are more pronounced in the *in-vitro* activated, stellate forms of rodent astrocytes that are induced by serum deprivation and maintenance in G5 cell culture supplement.

A still unresolved question pertains to the mechanism of P2X7 current run-up during repetitive ATP application, which was clearly evident in recombinant hP2X7, native hP2X7 and recombinant rP2X7 receptors, but not in rat or mouse astroglia cultures. P2X7 current run-up as well as the progressive delay in P2X7 current decay upon agonist removal appear to correlate with the pore dilation or sensitization process (Yan *et al.*, 2010), which may rely in part on the cellular background investigated. When expressed in *X. laevis* oocytes, pore dilation could not be detected with both rat and human P2X7 receptors (Petrou *et al.*, 1997; Klapperstück *et al.*, 2000). Similarly, hP2X7 current run-up was also absent in Müller glial cells from human retina (Pannicke *et al.*, 2000).

Taken together, the data imply that ivermectin adds to the growing list of species-specific P2X7 receptor modulators. Thus, ivermectin should be used with caution when probing P2X receptors on human cells and tissues. Although potentiation of native ATP-triggered conductances in human macrophages may suggest a role for ivermectin in stimulation of ATP-dependent immune responses, this hypothesis would require a more thorough analysis of ivermectin effects under pathophysiologically modified conditions.

Acknowledgements

This work was supported by the Deutsche Forschungsgemeinschaft (Scha 941/2 to MS and WN) within the framework of FOR 748.

Conflicts of interest

None.

References

Abramoff MD, Magalhaes PJ, Ram SJ (2004). Image processing with imageJ. Biophotonics International 11: 36–42.

Agboh KC, Webb TE, Evans RJ, Ennion SJ (2004). Functional characterization of a P2X receptor from *Schistosoma mansoni*. J Biol Chem 279: 41650–41657.

Alexander SPH, Mathie A, Peters JA (2011). Guide to receptors and channels (GRAC), 5th edition. Br J Pharmacol 164 (Suppl 1): S1–324.

Alloisio S, Aiello R, Ferroni S, Nobile M (2006). Potentiation of native and recombinant P2X7-mediated calcium signalling by arachidonic acid in cultured cortical astrocytes and human embryonic kidney 293 cells. Mol Pharmacol 69: 1975–1983.

Bavan S, Straub VA, Blaxter ML, Ennion SJ (2009). A P2X receptor from the tardigrade species *Hypsibius dujardini* with fast kinetics and sensitivity to zinc and copper. BMC Evol Biol 9: 17. doi: 10.1186/1471-2148-9-17.

Brône B, Moechars D, Marrannes R, Mercken M, Meert T (2007). P2X currents in peritoneal macrophages of wild type and $P2X_4^{-/-}$ mice. Immunol Lett 113: 83–89.

Burnstock G, Kennedy C (2011). P2X receptors in health and disease. Adv Pharmacol 61: 333–372.

Burnstock G, Verkhratsky A (2010). Long-term (trophic) purinergic signalling: purinoceptors control cell proliferation, differentiation and death. Cell Death Dis 1: e7.

Coddou C, Acuna-Castillo C, Bull P, Huidobro-Toro JP (2007). Dissecting the facilitator and inhibitor allosteric metal sites of the $P2X_4$ receptor channel: critical roles of CYS^{132} for zinc potentiation and ASP^{138} for copper inhibition. J Biol Chem 282: 36879–36886.

Coddou C, Yan Z, Obsil T, Huidobro-Toro JP, Stojilkovic SS (2011). Activation and regulation of purinergic P2X Receptor channels. Pharmacol Rev 63: 641–683.

Collins T, Millar NS (2010). Nicotinic acetylcholine receptor transmembrane mutations convert ivermectin from a positive to a negative allosteric modulator. Mol Pharmacol 78: 198–204.

Cully DF, Vassilatis DK, Liu KK, Paress PS, Van der Ploeg LH, Schaeffer JM *et al*. (1994). Cloning of an avermectin-sensitive glutamate-gated chloride channel from *Caenorhabditis elegans*. Nature 371: 707–711.

Davies JQ, Gordon S (2005). Isolation and culture of human macrophages. Methods Mol Biol 290: 105–116.

Dawson GR, Wafford KA, Smith A, Marshall GR, Bayley PJ, Schaeffer JM *et al*. (2000). Anticonvulsant and adverse effects of avermectin analogs in mice are mediated through the gamma-aminobutyric acid$_A$ receptor. J Pharmacol Exp Ther 295: 1051–1060.

Donnelly-Roberts D, McGaraughty S, Shieh CC, Honore P, Jarvis MF (2008). Painful purinergic receptors. J Pharmacol Exp Ther 324: 409–415.

Duan S, Anderson CM, Keung EC, Chen Y, Chen Y, Swanson RA (2003). P2X$_7$ receptor-mediated release of excitatory amino acids from astrocytes. J Neurosci 23: 1320–1328.

Edelstein A, Amodaj N, Hoover K, Vale R, Stuurman N (2010). Computer control of microscopes using μmanager. Curr Protoc Mol Biol DOI: 10.1002/0471142727.mb1420s92.

Fellin T, Pozzan T, Carmignoto G (2006). Purinergic receptors mediate two distinct glutamate release pathways in hippocampal astrocytes. J Biol Chem 281: 4274–4284.

Ferrari D, Pizzirani C, Gulinelli S, Callegari G, Chiozzi P, Idzko M *et al*. (2007). Modulation of P2X$_7$ receptor functions by polymyxin B: crucial role of the hydrophobic tail of the antibiotic molecule. Br J Pharmacol 150: 445–454.

Fischer W, Appelt K, Grohmann M, Franke H, Nörenberg W, Illes P (2009). Increase of intracellular Ca^{2+} by P2X and P2Y receptor-subtypes in cultured cortical astroglia of the rat. Neuroscience 160: 767–783.

Franke H, Günther A, Grosche J, Schmidt R, Rossner S, Reinhardt R *et al*. (2004). P2X$_7$ receptor expression after ischemia in the cerebral cortex of rats. J Neuropathol Exp Neurol 63: 686–699.

Giulian D, Baker TJ (1986). Characterization of ameboid microglia isolated from developing mammalian brain. J Neurosci 6: 2163–2178.

Guile SD, Alcaraz L, Birkinshaw TN, Bowers KC, Ebden MR, Furber M *et al*. (2009). Antagonists of the P2X$_7$ receptor. From lead identification to drug development. J Med Chem 52: 3123–3141.

Guo C, Masin M, Qureshi OS, Murrell-Lagnado RD (2007). Evidence for functional P2X$_4$/P2X$_7$ heteromeric receptors. Mol Pharmacol 72: 1447–1456.

Hibbs RE, Gouaux E (2011). Principles of activation and permeation in an anion-selective Cys-loop receptor. Nature 474: 54–60.

Hosie AM, Wilkins ME, da Silva HM, Smart TG (2006). Endogenous neurosteroids regulate GABA$_A$ receptors through two discrete transmembrane sites. Nature 444: 486–489.

Jarvis MF, Khakh BS (2009). ATP-gated P2X cation-channels. Neuropharmacology 56: 208–215.

Jelínkova I, Vávra V, Jindrichova M, Obsil T, Zemkova HW, Zemkova H *et al*. (2008). Identification of P2X$_4$ receptor transmembrane residues contributing to channel gating and interaction with ivermectin. Pflugers Arch 456: 939–950.

Junger WG (2011). Immune cell regulation by autocrine purinergic signalling. Nat Rev Immunol 11: 201–212.

Kawate T, Michel JC, Birdsong WT, Gouaux E (2009). Crystal structure of the ATP-gated P2X$_4$ ion channel in the closed state. Nature 460: 592–598.

Khakh BS, North RA (2006). P2X receptors as cell-surface ATP sensors in health and disease. Nature 442: 527–532.

Khakh BS, Bao XR, Labarca C, Lester HA (1999a). Neuronal P2X transmitter-gated cation channels change their ion selectivity in seconds. Nat Neurosci 2: 322–330.

Khakh BS, Proctor WR, Dunwiddie TV, Labarca C, Lester HA (1999b). Allosteric control of gating and kinetics at P2X$_4$ receptor channels. J Neurosci 19: 7289–7299.

Klapperstück M, Büttner C, Böhm T, Schmalzing G, Markwardt F (2000). Characteristics of P2X$_7$ receptors from human B lymphocytes expressed in *Xenopus* oocytes. Biochim Biophys Acta 1467: 444–456.

Lalo U, Pankratov Y, Wichert SP, Rossner MJ, North RA, Kirchhoff F *et al*. (2008). P2X$_1$ and P2X$_5$ subunits form the functional P2X receptor in mouse cortical astrocytes. J Neurosci 28: 5473–5480.

Lenertz LY, Gavala ML, Zhu Y, Bertics PJ (2011). Transcriptional control mechanisms associated with the nucleotide receptor P2X7, a critical regulator of immunologic, osteogenic, and neurologic functions. Immunol Res 50: 22–38.

Lynagh T, Webb TI, Dixon CL, Cromer BA, Lynch JW (2011). Molecular determinants of ivermectin sensitivity at the glycine receptor chloride channel. J Biol Chem 286: 43913–43924.

Martin RJ, Kusel JR (1992). On the distribution of a fluorescent ivermectin probe (4″ 5,7 dimethyl-bodipy proprionylivermectin) in Ascaris membranes. Parasitology 104: 549–555.

McGrath J, Drummond G, Kilkenny C, Wainwright C(2010). Guidelines for reporting experiments involving animals: the ARRIVE guidelines. Br J Pharmacol 160: 1573–1576.

Michel AD, Ng SW, Roman S, Clay WC, Dean DK, Walter DS (2009). Mechanism of action of species-selective P2X$_7$ receptor antagonists. Br J Pharmacol 156: 1312–1325.

Mihic SJ, Ye Q, Wick MJ, Koltchine VV, Krasowski MD, Finn SE *et al*. (1997). Sites of alcohol and volatile anaesthetic action on GABA$_A$ and glycine receptors. Nature 389: 385–389.

Nörenberg W, Schunk J, Fischer W, Sobottka H, Riedel T, Oliveira JF *et al*. (2010). Electrophysiological classification of P2X7 receptors in rat cultured neocortical astroglia. Br J Pharmacol 160: 1941–1952.

Nörenberg W, Hempel C, Urban N, Sobottka H, Illes P, Schaefer M (2011). Clemastine potentiates the human P2X7 receptor by sensitizing it to lower ATP concentrations. J Biol Chem 286: 11067–11081.

North RA (2002). Molecular physiology of P2X receptors. Physiol Rev 82: 1013–1067.

Oliveira JF, Riedel T, Leichsenring A, Heine C, Franke H, Krugel U *et al*. (2011). Rodent cortical astroglia express *in situ* functional P2X7 receptors sensing pathologically high ATP concentrations. Cereb Cortex 21: 806–820.

Pannicke T, Fischer W, Biedermann B, Schädlich H, Grosche J, Faude F *et al*. (2000). P2X$_7$ receptors in Müller glial cells from the human retina. J Neurosci 20: 5965–5972.

Petrou S, Ugur M, Drummond RM, Singer JJ, Walsh JV Jr (1997). P2X7 purinoceptor expression in *Xenopus* oocytes is not sufficient to produce a pore-forming P2Z-like phenotype. FEBS Lett 411: 339–345.

Priel A, Silberberg SD (2004). Mechanism of ivermectin facilitation of human $P2X_4$ receptor channels. J Gen Physiol 123: 281–293.

Silberberg SD, Li M, Swartz KJ (2007). Ivermectin Interaction with transmembrane helices reveals widespread rearrangements during opening of P2X receptor channels. Neuron 54: 263–274.

Vermeiren C, Najimi M, Maloteaux JM, Hermans E (2005). Molecular and functional characterisation of glutamate transporters in rat cortical astrocytes exposed to a defined combination of growth factors during *in vitro* differentiation. Neurochem Int 46: 137–147.

Virginio C, Church D, North RA, Surprenant A (1997). Effects of divalent cations, protons and calmidazolium at the rat $P2X_7$ receptor. Neuropharmacology 36: 1285–1294.

Wildman SS, King BF, Burnstock G (1999). Modulation of ATP-responses at recombinant rP2X4 receptors by extracellular pH and zinc. Br J Pharmacol 126: 762–768.

Wu T, Dai M, Shi XR, Jiang ZG, Nuttall AL (2011). Functional expression of P2X4 receptor in capillary endothelial cells of the cochlear spiral ligament and its role in regulating the capillary diameter. Am J Physiol Heart Circ Physiol 301: H69–H78.

Yan Z, Khadra A, Li S, Tomic M, Sherman A, Stojilkovic SS (2010). Experimental characterization and mathematical modeling of P2X7 receptor channel gating. J Neurosci 30: 14213–14224.

Yan Z, Khadra A, Sherman A, Stojilkovic SS (2011). Calcium-dependent block of P2X7 receptor channel function is allosteric. J Gen Physiol 138: 437–452.

Ye Q, Koltchine VV, Mihic SJ, Mascia MP, Wick MJ, Finn SE *et al.* (1998). Enhancement of glycine receptor function by ethanol is inversely correlated with molecular volume at position α267. J Biol Chem 273: 3314–3319.

Supporting information

Additional Supporting Information may be found in the online version of this article:

Figure S1 Ivermectin but not clemastine augments P2X4 currents and leads to a delayed current decay. Human P2X4 receptors were stably expressed (HEK_{hP2X4} cell line) and subjected to electrophysiological analysis in the whole-cell mode (holding potential –60 mV) in a bath solution containing low concentrations of divalent cations (low DIC; 0.1 mM $CaCl_2$, no added $MgCl_2$). Short pulses (2 s) of 3 μM ATP were applied three times (I_1 to I_3) at 3 min intervals to the cells in the presence or absence of 3 μM ivermectin (A,C) or 30 μM clemastine (B,C) added for the 3 min prior and during I_2. Insets in panels A and B depict a magnification of the normalized current traces in the decaying phase (right) and a statistical analysis of decay half-times ($T_{1/2}$) in the absence (I_1, t = 0 min), presence (I_2, t = 3 min) and after wash-out (I_3, t = 6 min) of the respective modulator (left). (C) Ratios of ATP-triggered P2X4 currents in the presence of ivermectin (I_2; n = 9) or clemastine (I_2; n = 11) compared with currents in the presence of ATP alone (I_1), and expressed as percentage of I_1.

Figure S2 Kinetic properties of the ivermectin-induced hP2X7 current potentiation. (A, a–c) ATP-induced currents in HEK_{hP2X7} cells were recorded during acute addition and removal of various concentrations of ivermectin as shown in Figure 4 of the main manuscript. Continuous lines represent bi-exponential fits of rise and decay times. Note that in all experiments, the major fraction (> 93%) of the reversible current augmentation during ivermectin application developed and decayed with a fast (τ_{fast}) time constant. A second, slow time constant (τ_{slow}), necessary only for adequately fitting the very late phase of current onset and decay, showed high cross-experimental variability (see panel A). (D) Aggregated data from n = 7–11 measurements (same set of experiments also shown in Fig 4A, B) as depicted in panels A–C reveal no significant interdependency of the respective fast components of the rise and decay time constants with variations of the ivermectin concentration.

Figure S3 Ivermectin does not induce hP2X7 currents in the absence of ATP. ATP-induced currents in HEK_{hP2X7} cells were allowed to develop, followed by application of ivermectin at the indicated concentrations but without ATP in the bath solution. At the end of each experiment, currents in the presence of ATP alone were re-analysed to verify the maintained responsiveness of hP2X7 receptors. ATP or ivermectin were applied in low DIC and at a holding potential of –60 mV for 6 s at 2 min intervals. (A) Repetitive stimulation with ATP caused an initial run-up of current amplitudes (superimposed responses to the first, sixth and seventh ATP application shown at the left). The dashed line designates the stage to which the ATP-induced current amplitudes grew. Note that ivermectin does not evoke membrane currents in the absence of ATP. (B) Statistical analysis of seven independent experiments as illustrated in panel A. Shown are mean current amplitudes ± SEM evoked by ATP or increasing concentrations of ivermectin without ATP.

Figure S4 Ivermectin potentiates hP2X7 currents in the same cell irrespective of whether they are activated by submaximally or maximally effective ATP concentrations. (A) ATP (300 μM)-induced currents in HEK_{hP2X7} cells were repetitively elicited until a steady state has developed (no difference between the sixth and the seventh pulse). Subsequently, hP2X7 currents were induced by saturating (10 mM) or submaximally effective (300 μM) ATP concentrations prior, during and after addition of 3 μM ivermectin to the bath solution. (B) Cumulative data of n = 9 independent experiments performed as shown in panel A. Asterisks denote significant ($P < 0.05$) increases in ATP-induced current densities in the presence of ivermectin compared with the corresponding ATP concentrations applied in the absence of ivermectin.

Figure S5 Effects of ivermectin on $[Ca^{2+}]_i$ signals in G5-activated rat astroglia. Astroglia cell suspensions were loaded with 4 μM fluo-4/AM, washed and pre-incubated with the indicated modulators for 5–10 min, followed by acute addition of 100 μM BzATP. (A) Time lapse analysis of fluo-4 florescence intensity during stimulation with BzATP. (B) Sensitivity of Ca^{2+} signals to sub-micromolar A 438079 concentrations (IC_{50} = 0.86 ± 0.12 μM; nH = 1.01 ± 0.09) hints to a major contribution of P2X7 receptors to the BzATP-induced signals in G5-treated rat astrocytes. BzATP-triggered fluorescence increases were normalized to signals observed in the absence of A 438079 (% of BzATP alone).

Shown are means ± SE of six determinations, accumulated in three independent experiments. (C) P2X7-like signals in rat G5-treated astroglia cultures are concentration-dependently potentiated by clemastine (eight determinations in four independent experiments; four determinations with A 438079). (D) Ivermectin effects were assessed and depicted as means ± SE of eight and six determinations (three to four independent experiments) in the absence and presence of 10 μM A 438079 respectively.

Figure S6 Ivermectin does not increase ATP-triggered currents in HEK cells stably expressing rat P2X7 receptors (HEK_{rP2X7}). (A) Whole-cell recordings were obtained at a holding potential of –60 mV and in a low DIC bath solution. ATP (300 μM) was applied 12 times for 6 s and at 2 min intervals. Shown are superimposed responses to the 1st, 11th and 12th challenge (left panel). After another 2 min, ATP was applied to the same cell for the 13th time, and ivermectin (3 μM) was added acutely 4 s after ATP application (see application bars). To compensate for secondary current growth, amplitudes without (I_1) or with (I_2) ivermectin were quantified 6 s after ATP application. (B) Time course of rP2X7 current run-up in recombinant rat P2X7 receptors. Current amplitudes were measured after 6 s in ATP (I_1 in A, left panel). Note the steady state of I_1 that was reached with the 11th challenge by ATP. (C) Bars represent aggregated data (means ± SE) of $n = 8$ independent experiments performed as shown in panel A.

Please note: Wiley-Blackwell are not responsible for the content or functionality of any supporting materials supplied by the authors. Any queries (other than missing material) should be directed to the corresponding author for the article.